Stratigraphic architecture of fluvial fans shaped by downstream changes in avulsion style

Valenza, Jeffery M.; Edmonds, Douglas A.; Martin, Harrison K.; Sifuentes, Caitlin; Toby, Stephan

DOI
10.1111/sed.13217

Publication date
2024

Document Version
Final published version

Published in
Sedimentology

Citation (APA)
Valenza, J. M., Edmonds, D. A., Martin, H. K., Sifuentes, C., & Toby, S. (2024). Stratigraphic architecture of fluvial fans shaped by downstream changes in avulsion style. *Sedimentology*, *71*(7), 2335-2357. https://doi.org/10.1111/sed.13217

SEDIMENTOLOGY the journal of the International Association of Sedimentologists IAS

Sedimentology (2024) **71**, 2335–2357 doi: 10.1111/sed.13217

Stratigraphic architecture of fluvial fans shaped by downstream changes in avulsion style

JEFFERY M. VALENZA*,†, DOUGLAS A. EDMONDS†, HARRISON K. MARTIN†,‡, CAITLIN SIFUENTES† and STEPHAN TOBY†,§

**Department of Geography, University of California, 1832 Ellison Hall, Santa Barbara, CA 93106, USA (E-mail: jeffvalenza@gmail.com)*

†Department of Earth and Atmospheric Sciences, Indiana University, 1001 E 10th St., Bloomington, Indiana 47405, USA

‡Division of Geological and Planetary Sciences, California Institute of Technology, 1200 E California Blvd., Pasadena, California 91125, USA

§Department of Geoscience and Engineering, TU Delft, Stevinweg 1, Building 23 2628CN, Delft, The Netherlands

Associate Editor – Massimiliano Ghinassi

ABSTRACT

Natural river diversion, or avulsion, controls the distribution of channels on a floodplain and channel sandstone bodies within fluvial stratigraphic architecture. Avulsions establish new flow paths and create channels through several recognized processes, or styles. These include reoccupying existing channels, or annexation, downcutting into the floodplain, or incision, and constructing new channels from crevasse-splay distributary networks, or progradation. Recent remote sensing observations show that avulsion style changes systematically moving downstream along modern fluvial fans but, to date, no studies have assessed the significance of these trends on fluvial fan stratigraphy. Here, spatiotemporal changes in avulsion stratigraphy are investigated within the Salt Wash Member of the Morrison Formation, deposited in the Cordilleran foreland basin during the Late Jurassic epoch. Measured sections and photographic panels were analysed from 23 locations across the Salt Wash extent. Avulsion style was identified in the stratigraphic record by the basal contact of a channel storey with underlying strata: channel–channel contacts indicate annexation, channel–floodplain contacts indicate incision and channel–heterolithic contacts indicate progradation. Contact types change downstream, such that channel–channel and channel–floodplain contacts dominate proximal locations, while channel–heterolithic contacts become increasingly prevalent downstream. Outcrop results were compared to a numerical model of fluvial fan formation and remote-sensing analysis of avulsions on modern fans. In both additional datasets, channels in proximal fan positions tend to avulse via annexation, reoccupying abandoned channels, while channels in more distal positions tend to avulse via increasingly significant progradation. These findings suggest a relationship between newly recognized downstream changes in avulsion style and well-established downstream changes in fluvial fan architecture. Furthermore, this suggests that fan architecture can inform interpretations of ancient fluvial dynamics, including avulsion behaviour, and that avulsions can cause stratigraphically significant and measurable changes to fan architecture.

Keywords Annexation, avulsion, fan, fluvial, model, Morrison Formation, progradation, stratigraphy.

INTRODUCTION

The wholesale avulsion of river channels constitutes one of the most important processes for building fluvial stratigraphy. During avulsion, the channel repositions itself on the floodplain. Over time, avulsions determine the distribution and stacking patterns of channel sand bodies and associated overbank sediment packages deposited by active channels (Allen, 1965, 1978; Bridge & Leeder, 1979). Thus, avulsions represent episodic depositional events that contribute directly and indirectly to floodplain aggradation as channels shift to entirely new locations. The frequency, location and behaviour (or style) of avulsion events reflect important depositional and environmental conditions such as channel aggradation rates and floodplain hydrological connectivity (Slingerland & Smith, 1998; Jones & Schumm, 1999; Aslan *et al.*, 2005).

Avulsions have been categorized into three distinct styles based on how channel flow is reestablished after an initial diversion (Smith *et al.*, 1989; Slingerland & Smith, 1998, 2004; Mohrig *et al.*, 2000). The first of these styles describes the diversion of flow directly into a pre-existing channel, which effectively annexes a nearby flow path. In the absence of significant downcutting or reworking of the previous channel sediments, annexational style avulsion would result in a multi-storey sand body, where each subsequent storey represents one channel occupation at that location (Chamberlin & Hajek, 2015). The second style includes events in which diverted flow incises significantly into the floodplain, erasing any pre-existing channel deposits and producing an isolated sand body surrounded by floodplain sediments. Such incisional avulsions are difficult to identify in modern systems without sediment coring, but in the rock record they are identified as channel sandstone bodies that make direct contact along most of the channel–storey margin with underlying and genetically unrelated fine-grained floodplain sediments (Slingerland & Smith, 2004; Jones & Hajek, 2007). The third avulsion style occurs when flow is diverted onto the floodplain and progresses downstream through a complex series of crevasse splays (Millard *et al.*, 2017). These progradational avulsions resolve as advancing crevasse-splays form a new channel capable of transporting the diverted discharge (Smith *et al.*, 1989; Smith & Perez-Arlucea, 1994; Perez-Arlucea & Smith, 1999; Morozova & Smith, 2000; Slingerland & Smith, 2004).

Traditionally, most measures of avulsion stratigraphy have focused on how channel–storey stacking patterns change through time by looking at vertical changes in the distribution of channel sandstone bodies in outcrop or in pseudo-stratigraphy produced by numerical models (Allen, 1965, 1978; Leeder, 1977; Bridge & Leeder, 1979; Rust & Jones, 1987; Bryant *et al.*, 1995; Heller & Paola, 1996; Holbrook, 2001; Gibling, 2006; Labourdette & Jones, 2007; Hajek & Wolinsky, 2012; Chamberlin & Hajek, 2015; Chamberlin *et al.*, 2016). However, few studies have investigated how avulsion style changes through space and time within a particular system. For instance, case studies describing avulsion stratigraphy in specific geological formations typically generalize formations as hosting a dominant avulsion style, such as progradation-dominated (Fort Union Formation, Kraus & Wells, 1999; Willwood Formation, Kraus & Gwinn, 1997, and Jones & Hajek, 2007) or incision-dominated (Ferris Formation, Jones & Hajek, 2007). The Shire Member of the Wasatch Formation has been quantitatively characterized as hosting both progradational (57%) and incisional (43%) avulsion indicators (Foreman *et al.*, 2012; Hajek & Edmonds, 2014), but no spatiotemporal trends in avulsion behaviour were reported.

Recent remote sensing analysis has yielded novel insight into the distribution of avulsion processes across foreland fluvial systems. Valenza *et al.* (2020, 2022) identified correlations between avulsion style and channel morphology, slope and distance from the foreland margin or fan apex. These studies observed that avulsion events occurring in proximity to fan apices were annexation dominated, and that those occurring more distally were dominated by progradational processes. While these trends were observed across multiple basins, the remote-sensing approach precluded any definitive assessment of their stratigraphic significance.

To this end, the Salt Wash Member of the Morrison Formation was selected as a test case due to excellent preservation and outcrop exposure, well-documented stratigraphy, and detailed interpretations of the system's depositional history (Weissmann *et al.*, 2013; Owen *et al.*, 2015a,b, 2017). Observations were framed within the geomorphic succession synthesized by Hartley *et al.* (2010) from a global survey of distributive fluvial systems. In this framework, a fan system is divided into a radially distributive

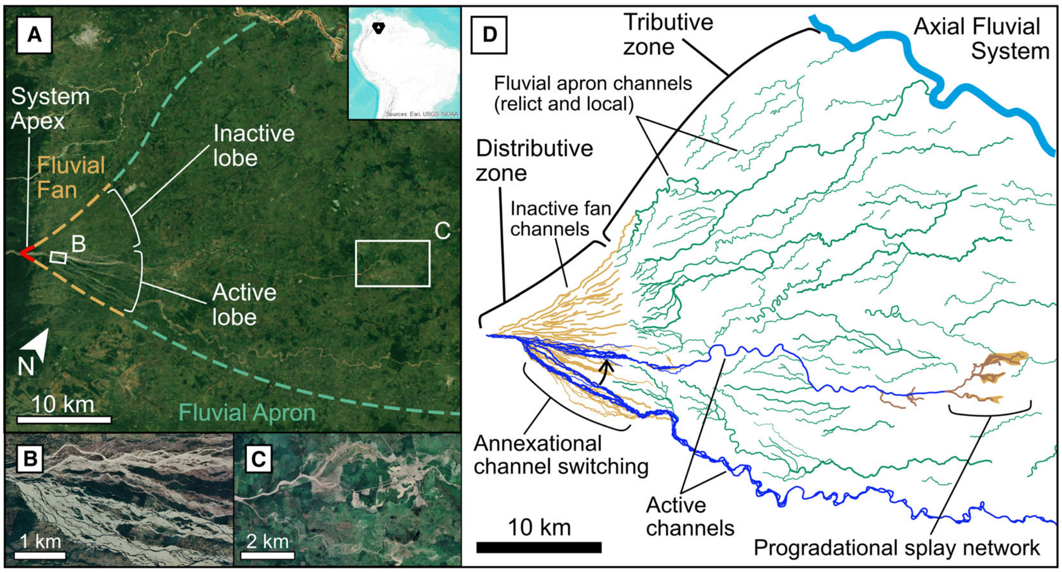

Fig. 1. Active fluvial fan system, Arauca Department, Colombia. (A) The fan apex, located at the basin margin, feeds the fluvial fan, which hosts a dense radial distribution of mostly abandoned channels. Downstream, the fan transitions to a fluvial apron, which hosts local drainage systems that are distinguished from the fan by their tributive channel arrangements. (B) Detail of radially distributed fluvial fan channels. (C) Detail of prograding avulsion splay network on the fluvial apron. (D) Line diagram of the fan-apron system highlighting distinct channel organization in the proximal distributive zone (fan) and the medial to distal tributive zone (apron). Note high distribution density of channels on the fan, compared to much lower channel density on the apron. Imagery source: Google Earth Pro (2024), (6.691150° N, 71.846373° W).

fluvial fan, which transitions downstream to a tributive apron, which then transitions into or joins the basin's axial drainage system (Fig. 1). Avulsion behaviour, depositional environment and stratigraphic architecture are related by framing stratigraphic descriptors of proximal and medial depositional zones in terms of fluvial fan processes, and those of the distal zone in terms of fluvial apron processes.

Outcrop observations are compared to simulated avulsion activity in a numerically modelled fluvial fan (Martin & Edmonds, 2022, 2023), and to remote-sensing analysis of avulsions on several modern fluvial fan–apron systems. Evidence of downstream changes in avulsion style are found in the Salt Wash Member, the numerical model and the remote-sensing record. Salt Wash alluvial architecture changes downstream and up-section from a channel-dominated to floodplain-dominated regime, accompanied by a shift from predominantly annexational and incisional to progradational avulsion behaviour. These two regimes occur in distinct spatiotemporal zones, which are consistent with the results of the fluvial fan model, which predicted greater progradational distances in distal reaches. Furthermore, both outcrop and model results are consistent with remote-sensing observations from modern settings. Identifying and characterizing the stratigraphic indicators of this downstream shift reveals a channel-scale, morphodynamic mechanism for spatiotemporal changes in the stratigraphic architecture of fluvial fan systems.

DEPOSITIONAL AND TECTONIC HISTORY OF THE MORRISON FORMATION

The Morrison Formation represents a predominantly fluvial succession deposited across the Cordilleran retroarc foreland basin of North America during the late Jurassic (Kowallis *et al.*, 1998; Turner & Peterson, 2004) (Fig. 2A). Throughout the Mesozoic era, western North America experienced a chiefly north-west to south-east compressional tectonic regime as the Farallon oceanic plate subducted beneath the western margin of North America (DeCelles, 2004; Dickinson, 2004). The Morrison Formation was deposited between 155 Ma and 148 Ma,

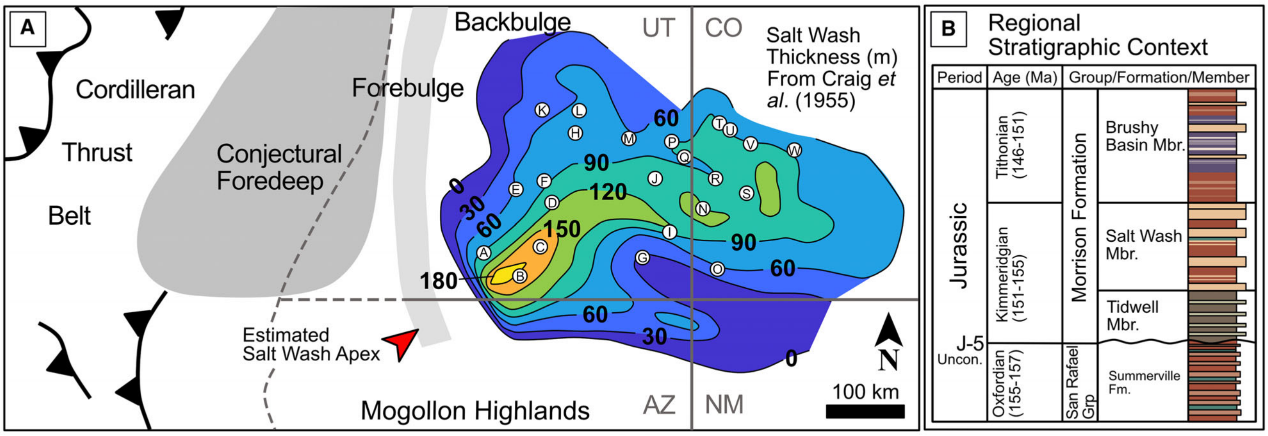

Fig. 2. Tectonic and stratigraphic settings of the Morrison Formation. (A) Salt Wash Member sediments were deposited in the backbulge of the Cordilleran Foreland Basin, across what is now the modern-day Colorado Plateau. Red arrow marks estimated Salt Wash system apex (Owen *et al.*, 2015a), lettered circles mark outcrop locations, and thickness contours are mapped at 30 m intervals. (B) The Morrison Formation alternates between the poorly drained floodplains of the Tidwell Member to the well-drained, channel-dominated Salt Wash Member, back to the floodplain-dominated Brushy Basin Member (Peterson, 1980; Robinson & McCabe, 1998).

before or during the initial phases of the Sevier Orogeny (Kowallis *et al.*, 1991, 1998; DeCelles & Burden, 1992; DeCelles & Currie, 1996; DeCelles, 2004; Dickinson, 2006). This period was marked by local thrust-deformation in Northern Utah and Nevada (Allmendinger *et al.*, 1984) and thermogenic uplift of the Cordillera to the west (Heller *et al.*, 1986). The basin was flanked to the south by the Mogollon Highlands, an elevated rift shoulder related to the Bisbee–McCoy strike-slip rift basin, also oriented north-west to south-east (Dickinson & Lawton, 2001; Spencer *et al.*, 2011). This tectonic setting contributed to late Jurassic subsidence of the Cordilleran foreland, especially to the west and north of the modern Colorado Plateau, creating the greatest accommodation to the east and south of the preserved extent of the Morrison Formation. Thus, preserved and exposed Morrison sediments are thought to have been deposited in a low accommodation setting, either due to overfilling of the foredeep or due to flexural uplift of a pronounced forebulge (Peterson, 1984; DeCelles & Burden, 1992; DeCelles & Currie, 1996; Currie, 1997; DeCelles, 2004).

Across most of Utah and western Colorado, the Morrison Formation is comprised of three members: the Tidwell, Salt Wash and Brushy Basin (Peterson, 1980; Robinson & McCabe, 1998) (Fig. 2B). The Tidwell Member hosts thin channel and overbank deposits within significant floodplain muds and muddy carbonate and evaporite lacustrine deposits (Peterson, 1980, 1994; Robinson & McCabe, 1998; Owen *et al.*, 2015b). The Salt Wash Member is the coarsest-grained and most channel-dominated of the three members, although the member becomes much more floodplain dominated towards the north-east (Craig *et al.*, 1955; Mullens & Freeman, 1957; Tyler & Ethridge, 1983). The Brushy Basin Member hosts the thickest successions of floodplain muds in colourful palaeosols interrupted by an occasional channel sandstone body (Peterson, 1980; Turner & Fishman, 1991; Demko *et al.*, 2004; Turner & Peterson, 2004). The Tidwell–Salt Wash transition is marked by the first large (>1 m thick) channel sandstone body, and the Salt Wash–Brushy Basin transition is generally marked by the first major succession of floodplain palaeosols separating channel sandstone bodies (Peterson, 1980). This transition becomes less distinct as the ratio of channel-to-floodplain facies in the Salt Wash decreases basinward (Owen *et al.*, 2015b, 2017).

Provenance and palaeoflow studies place the early Morrison watershed to the south-west of the Colorado Plateau (Peterson, 1986), either partly or wholly within the Mogollon Highlands (Dickinson & Gehrels, 2008), or at the syntaxis of the Sevier Orogenic Belt and the Mogollon Highlands (Owen *et al.*, 2015a). With a total observed area of *ca* 100 000 km^2, the Salt Wash Member ranges from 180 m thick at the most proximal outcrop, 50 Mile Point, south-west

Utah, to 40 m thick at Smith Fork, north-west Colorado (Weissmann *et al.*, 2013; Owen *et al.*, 2015a).

A radial distribution of palaeoflow indicators (Craig *et al.*, 1955; Mullens & Freeman, 1957; Robinson & McCabe, 1997) has been used to interpret the Salt Wash as a single system that distributed sediment from the modern south-west to the north–north-east. Using palaeoflow indicators from across the Salt Wash extent, Owen *et al.* (2015a) performed a statistical analysis to estimate the location of the system apex in north-western Arizona (Fig. 2A). Furthermore, Owen *et al.* (2015b) showed that the percentage of channel facies and average grain size both decrease in a radial pattern towards the north-east from the estimated apex location. That study characterized proximal, medial and distal facies assemblages, and identified a downstream migration of these facies assemblages through time, interpreting a progradation of the Salt Wash fluvial fan (see also Hartley *et al.*, 2010; Weissmann *et al.*, 2010, 2011; Owen *et al.*, 2017).

STRATIGRAPHIC AVULSION INDICATORS

Previous efforts by Kraus *et al.* (1999), Jones & Hajek (2007) and Chamberlin & Hajek (2015) identified various stratigraphic indicators of river avulsion and their connection to different processes. Kraus *et al.* (1999) drew from the modern Saskatchewan River avulsion, recent Colorado River deposits, and the Fort Union, Willwood and Chinji formations to develop a list of avulsion-related stratigraphic features. These included heterolithic sediment packages composed of alternating ribbon channel sands, sand sheets, and only weakly pedogenically altered muds, associated with a channel sandstone body and found directly below or lateral to it. Heterolithic packages exhibit extensive lateral continuity, representing depositional events that contributed a significant amount of sediment to the stratigraphic succession.

Jones & Hajek (2007) simplified this detailed set of criteria and presented an avulsion indicator scheme that is applicable to a broader range of fluvial systems and outcrop exposures. This scheme divided avulsion deposits into two general categories, determined by the nature of the stratigraphy at the base of channel sandstone bodies. Bodies emplaced directly atop pedogenically modified floodplain deposits, with little to no evidence of coarser-grained overbank deposition, are considered stratigraphically abrupt, indicating incision. This, in turn, can represent either the direct downcutting of diverted flow into the floodplain, or the annexation of a smaller channel which adjusted to increased discharge by deepening and erasing previous channel deposits (Slingerland & Smith, 2004). Alternatively, bodies overlying heterolithic overbank packages are considered stratigraphically transitional, indicating progradational avulsion.

The previous two schemes deal with avulsions that divert the channel onto the floodplain, resulting in isolated channel sandstone bodies emplaced by incision or progradation. Chamberlin & Hajek (2015) provided criteria for identifying avulsion activity in amalgamated or stacked channel sandstone bodies. Such multi-storey bodies can result from intra-channel, non-avulsion related processes such as intra-belt channel thread migration and meander cutoff (Johnson & Pierce, 1990; Platt & Keller, 1992; Leleu *et al.*, 2009; Corbett *et al.*, 2011), bar migration (Diemer & Belt, 1991; Kumar, 1993; Labourdette & Jones, 2007) and even seasonal fluctuations in discharge (Tunbridge, 1981; Olsen, 1989). The stratigraphy of avulsion-related multi-storey sandstone bodies differs from that of intra-channel ones in two important ways. First, along the erosional surface there may be fine-grained sediments deposited during or after abandonment. Second, avulsion-related storeys exhibit stepped or ‘sawtooth’ margins, indicating that the channel avulsed away from this position for a sufficient length of time for measurable floodplain sediment to accumulate before the channel returned and resumed development of levée deposits through overbank deposition of coarser-grained sediments. These sawtoothed edges of channel belts would not occur during smaller-scale cutoffs or the filling of an incised valley.

CHARACTERIZING AVULSION STRATIGRAPHY

Site selection

The Salt Wash Member was selected because it has been interpreted as a fluvial fan with an estimated palaeo-apex location (Owen *et al.*, 2015a) and has well-documented facies distributions (Owen *et al.*, 2015b). Sixteen locations

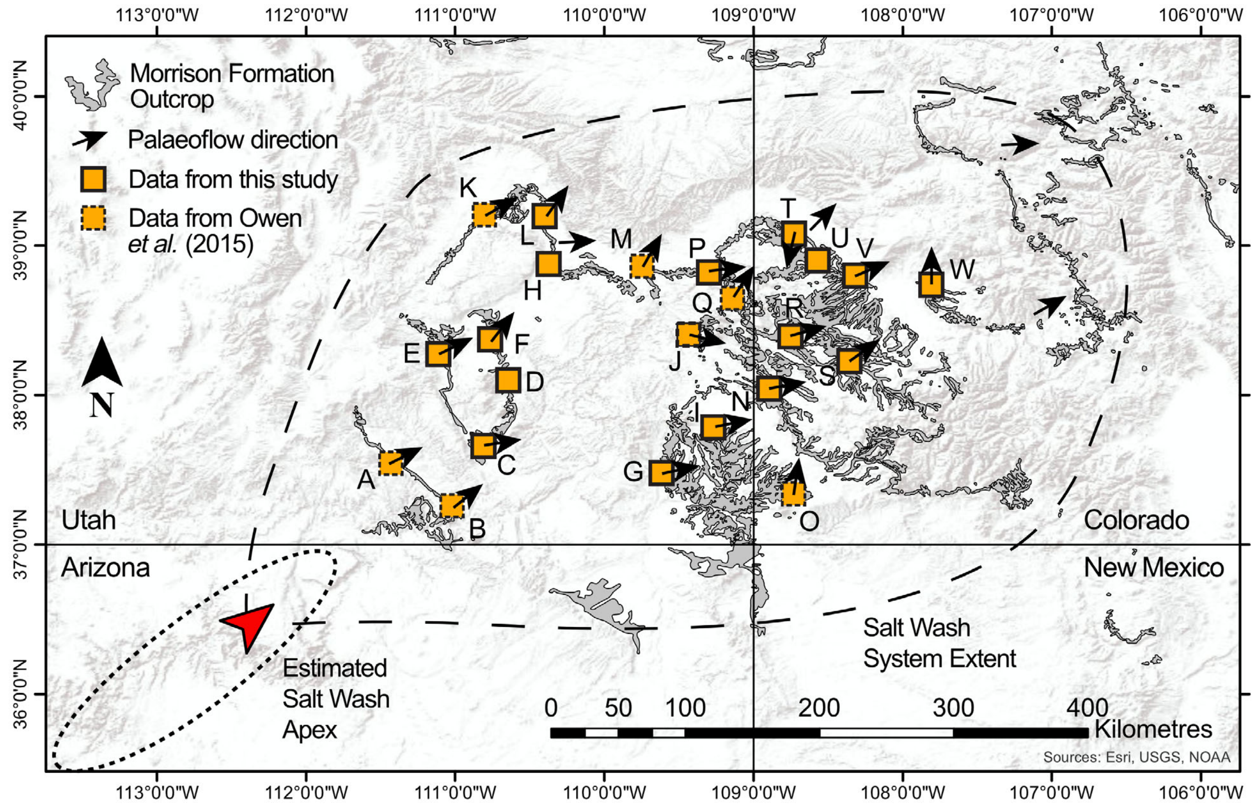

Fig. 3. Study locations and Salt Wash system extent. Gold markers indicate studied outcrop locations, and arrows mark mean palaeocurrent directions (Owen *et al*., 2015a). Grey fields indicate Morrison Formation outcrop and the dashed line is the Salt Wash system extent (Craig *et al*., 1955; Mullens & Freeman, 1957). Red arrow and dashed circle show estimated Salt Wash apex from Owen *et al*. (2015a).

across the Salt Wash Member (Fig. 3) were examined and correspond to sites described by Owen *et al*. (2015b). At each site, the basal contact of the Salt Wash Member with the underlying Tidwell Member was first identified. The outcrop face that would provide the fullest stratigraphic perspective was selected and captured through wide-angle photographic panels (Fig. 4A). Measurement at each site was concluded after the last channel sandstone body gave way to thick (tens of metres) successions of the colourful palaeosols of the overlying Brushy Basin Member. Geographical gaps between these outcrops were filled using an additional seven stratigraphic logs from Owen *et al*. (2015b) (Fig. 3).

Mapping stratigraphic avulsion indicators

Counting channel storeys

At each study site, channel sandstone bodies were identified, defined as ledge and cliff-forming, cross-bedded sandstone packages with metre-scale thicknesses and 10^2 to 10^3 metre-scale widths. Next, internal channel–storey boundaries were identified, including sawtoothed lateral margins (*sensu* Chamberlin & Hajek, 2015), mudplugs and through-going erosional surfaces.

Sawtoothed channel margins were identified as distinct extensions of sandy overbank or levée facies into the surrounding floodplain or overbank material from a channel storey (see fig. 2 from Chamberlin & Hajek, 2015). These margins were interpreted as indicators of annexation or reoccupation and thus as separate storeys. Sawtoothed margins result from prolonged periods of channel abandonment during which fine-grained floodplain sediments accumulated on the margins of the abandoned channel; upon reoccupation, these sediments were capped again by sandy deposits of the new channel and its levées. This alternation creates a sawtooth-shaped boundary along the margin of a multi-storey

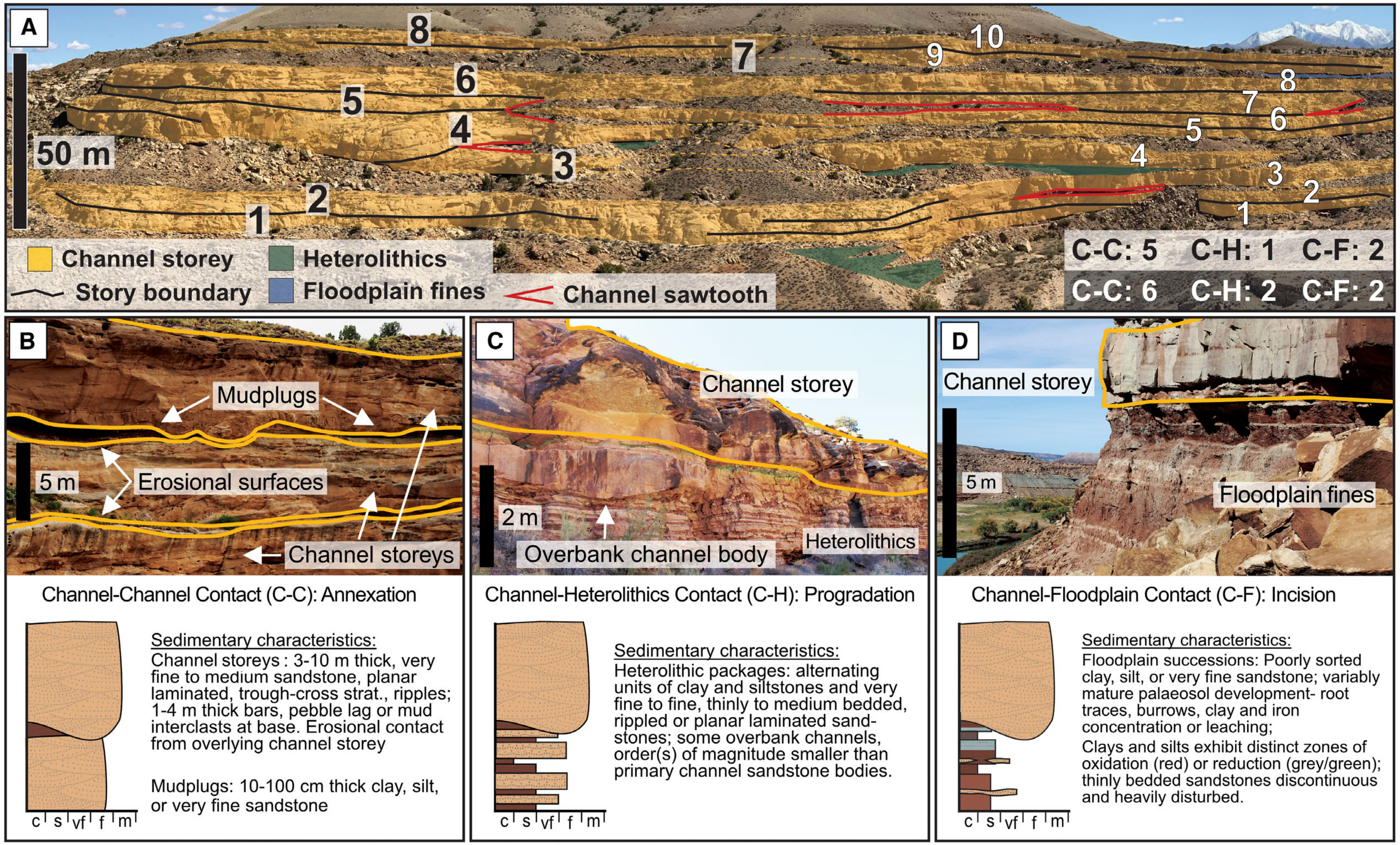

Fig. 4. Outcrop expression of stratigraphic avulsion indicators. (A) Photographic panel of channel–storey contacts from Henries outcrop (location D). Where an outcrop face hosted two distinguishable clusters of channel sandstone bodies, each was counted and categorized separately (left side in black lettering, right side in white), then characteristic values for that location were estimated by averaging values from each cluster together. (B) Channel–channel contacts, or C-C, are defined as channel storey bases contacting another channel storey – this may include mudplugs or channel facies. These contacts are used as indicators of annexational avulsion. (C) Channel–heterolithic contacts, or C-H, are defined as channel storey bases contacting alternating, thinly bedded sandstones, siltstones and mudstones. Heterolithics that exhibit intense weathering and bioturbation are considered mature palaeosols and categorized as floodplain material. These contacts are used as indicators of progradational avulsion activity. (D) Channel–floodplain contacts, or C-F, are defined as channel storey bases contacting fine-grained floodplain deposits. These may exhibit varying degrees of palaeosol maturity but must host predominantly silts and clays. These contacts are used as indicators of incisional avulsion.

sand body (Mackey & Bridge, 1995; Chamberlin & Hajek, 2015).

The lateral margins of multi-storey sand bodies were often not visible at the outcrop scale; in these cases, analysis was focused on basal channel–storey contacts, rather than sawtoothed margins. Storeys were identified within channel sandstone bodies by the presence of thinly bedded muddy units disrupting successions of otherwise homogeneous channel sand facies. These muddy units, interpreted as remnant mudplugs, consisted of isolated units of mud located between the upper contact of an underlying channel sandstone body and the basal, erosive contact of an overlying channel sandstone body. These muddy units ranged from several centimetres to *ca* 1 m thick and usually showed evidence of palaeosol development such as clay and iron concentrating soil horizons, root traces and coalified plant material (Li & Bhattacharya, 2014). Mudplugs were identified as facies associated with channel abandonment or subsequent floodplain deposition. In most cases, mudplugs are only present in scattered pockets between two channel storeys, because the upper channel can erode into the lower storey (Lynds & Hajek, 2006). Rare examples of isolated mud units, such as fine-grained pockets on the lee-side of dunes or bar clinoforms within channel facies, were not associated with a through-going erosional surface and were thus not used as channel–storey indicators.

Lastly, in the absence of sawtoothed margins or mudplugs, potential storey boundaries were identified using through-going erosional surfaces marked by clear breaks in sandy, cross-bedded channel facies (Chamberlin & Hajek, 2015). These features provide less reliable storey boundaries, however, because they can result from channel processes unrelated to avulsion, as previously mentioned. Storeys were interpreted from these surfaces when they extended through more than half of the exposed channel sandstone body and defined potential storeys scaling with sawtooth or mudplug-defined storey thicknesses elsewhere at the same outcrop. An entire channel sandstone body was interpreted as a single-storey if there were no breaks in cross-bedded sandstone facies and the body demonstrated basal and upper contacts with non-channel facies or fine-grained talus slopes.

Once all channel storeys were identified, their thicknesses were averaged to estimate a characteristic storey thickness for each outcrop. Minor channel sandstone bodies, or those two orders of magnitude narrower and two to five times thinner than major bodies, were not included. Furthermore, minor channel sandstone bodies were typically lens-shaped and lacked evidence of any type of channel migration common among the larger channels. These minor channel sandstone bodies were interpreted as parts of crevasse-splay complexes or as channels draining small, local regions of the floodplain.

Basal channel–storey contacts

Once all of the individual storeys were identified, basal contacts between each channel storey and the underlying facies were characterized. Classes of basal channel–storey contacts include channel–channel (C-C), channel–floodplain (C-H) and channel–heterolithic (C-F) (Fig. 4B to D). The following paragraphs describe and define the characteristic features of each type of contact.

Channel–channel contacts. These contacts are marked by the direct contact between an overlying and underlying channel storey (Fig. 4B). These storeys were recognized as thick packages of channel facies, composed of sandy dune and ripple cross-beds. In many cases, bar forms were partially preserved. A storey was interpreted as demonstrating a C-C contact, indicating annexational avulsion, if it contacted another channel storey over at least about one-third of its exposed base. In most cases, these channel storeys were in contact for more than half of their exposure. C-C contacts that can be traced laterally to a sawtoothed channel margin represent the highest-certainty avulsion indicator. Storeys making basal contacts with the mudplug of an underlying channel storey were also considered C-C contacts.

Channel–heterolithic contacts. These basal contacts describe contacts between channel storeys and heterolithic sediment packages (Fig. 4C). Heterolithic packages were identified as distinct successions of alternating sand and mud units. Channel-related, or overbank, heterolithic packages were distinguished from undifferentiated floodplain packages using sand content and palaeosol maturity. Heterolithic packages were defined as intervals of undisturbed, interbedded sand and mudstone bounded by either a channel sandstone body and/or more than 1 m of fine-grained floodplain material. Such intervals were interpreted as locally relevant and avulsion-related when they were in direct, underlying contact with channel sandstone bodies, and exhibited sandstone volumes of 20% or more. This threshold provided a clear difference in concentration of coarser-grained beds from typical floodplain packages, which hosted irregular and sparsely distributed 5 to 15 cm sandstone beds. Furthermore, to be used as an indicator of progradation-related overbank deposition, the heterolithic package needed to be relatively undisturbed by pedogenic alteration, such as bioturbation or iron and clay concentration. A contact was interpreted as C-H if it contacted heterolithic material over at least one-third of the exposed base.

The connection between C-H contact type and avulsion style can be ambiguous because the heterolithic package may not be genetically related to the channel storey. This scenario is considered unlikely, as no clear evidence of deep incision was observed throughout the study area. Furthermore, C-H contacts were only interpreted if there was minimal palaeosol development in the underlying heterolithic package, which maximizes the likelihood of a contemporary and, to a lesser extent, genetic, relationship. The lack of palaeosol development in the heterolithic unit is a key observation because it indicates that the heterolithic deposits were rapidly buried, which would likely occur during progradation (Morozova & Smith, 2000; Slingerland & Smith, 2004; Jones & Hajek, 2007). This kind of contact indicates that the depositional regime immediately prior to the emplacement of the channel storey produced overbank deposits, a characteristic but not exclusive feature of progradational avulsion activity. Ideally, a channel sandstone body emplaced through progradational activity would exhibit lateral contact with heterolithic facies that are remnants of the progradation event.

Channel–floodplain contacts. Ideally, these contacts are marked by the direct contact of a channel storey with underlying floodplain palaeosols, and the absence of a C-C or C-H contact elsewhere along the base of the storey (Fig. 4D). While channel sandstone bodies were easily identifiable throughout the study area as ledge or cliff-forming successions of channel facies, finer-grained strata were often less-exposed due to their less-resistant nature, resulting in talus and vegetation cover. Such cover likely represents the absence of sandstone because even minor channels or medium bedded units in heterolithic packages (10 cm to 1 m) were exposed through slope cover. In other cases, no observable stratigraphy was exposed below a particular channel sandstone body across the entire outcrop exposure. In cases where the base of the channel storey abutted slope cover, the interpretations of Owen *et al.* (2015b, 2017) were followed, which assume underlying, fine-grained, slope-forming floodplain facies. This contact type, indicating incisional avulsion, is effectively defined by the absence of the previous two contact types, and thus recognized as the least-certain avulsion indicator.

Contact-type analysis

The previous sections describe the steps and criteria for identifying channel sandstone bodies, defining channel storeys, and identifying avulsion indicators through the classification of basal channel–storey contacts. Most outcrops hosted few channel sandstone bodies that were exposed laterally from margin to margin, and bodies were most often distributed across exposures in loosely-defined clusters. To ensure that the maximum number of channel storeys at each outcrop were incorporated into the dataset, channel counts and contact characterizations were conducted for every storey at each location. In six locations, outcrops were wide enough to expose two clusters with several interfingered or shared channel sandstone bodies (for example, right and left sides of outcrop in Fig. 4A; locations E, H, G, C, M and R), storeys were characterized within both clusters, then cluster values were averaged to obtain a cumulative storey thickness, storey count and contact-type count for the outcrop. When channel sandstone bodies extended into more than one cluster, they were counted and characterized as observed in each cluster. Finally, channel sandstone bodies in contact with Tidwell Member stratigraphy were excluded from storey contact classification.

Owen *et al.* (2017) observed consistent upward coarsening of Salt Wash stratigraphy across its entire extent and interpreted these changes as evidence of basin-scale progradation of the ancient fluvial system. This interpretation provided context in which temporal changes in channel sandstone body characteristics could be identified. In the absence of chronologically correlative surfaces extending throughout the Salt Wash Member, this study opted for a straightforward division of each outcrop at its vertical midway point to approximate younger and older sections.

DISTRIBUTION OF AVULSION INDICATORS

Stratigraphic measurements from the Salt Wash Member

In total, 200 channel storeys were measured at 23 locations across the Salt Wash Member. Table 1 shows the distribution of channel storey contacts as a percentage of each type to assess the relative significance of the different avulsion indicators within the spatial extent of the Salt Wash Member (see Table S1 for full data set).

Channel–storey count and cumulative thickness

Outcrops hosting the greatest number of channel storeys are roughly aligned with the central axis of the Salt Wash system, extending from a maximum of twelve storeys at Fifty-Mile Canyon (B) to the north-east as far as Dewey Bridge (P), which hosted ten storeys (Fig. 5A). This trend is visible in both the lower and upper sections, with a north-west shift in storey concentration over time (Fig. 5B and C). Locations beyond this axial zone hosted significantly fewer storeys. Trends in cumulative storey thickness (Fig. 5D to F) generally follow those in storey count, where cumulative thickness is highest in proximal locations and, to a lesser extent, along a central axis, shifting from south-east to north-west over time. A maximum cumulative storey thickness of 122 m at Bullfrog (C) trends towards Polar Mesa (Q) and Atkinson Creek (R). Comparing outcrop panels from proximal (Bullfrog, C), medial (Butler Wash, G) and distal (Bangs Canyon, U) locations (Fig. 6) highlights a general downstream shift from thick, amalgamated channel sandstone bodies to more isolated, single-storey channel sandstone bodies encased in floodplain mud, which was also reported by Owen *et al*. (2015b, 2017).

Channel–storey contacts

Trends in the distribution of channel-storey contacts appear in both space and time. Assessed as a whole, the Salt Wash contains 28.3% C-C contacts, 37.5% C-H contacts and 25.9% C-F contacts, indicating a relatively even mix of contact types. In terms of areal distribution, the eight most proximal outcrops (A, C-G and I) host predominantly C-C and C-F storey contacts (Fig. 7A). This proximal zone also aligns generally with outcrops hosting above average storey thicknesses and numbers (6.3 m and 7.2 m, respectively). The medial zone shows no dominant type, whereas the distal zone is dominated by C-H storey contacts, except for several outcrops along a north-east-extending zone of relatively thicker and more numerous channel storeys (P, Q, R, U and V).

When breaking up the Salt Wash Member into upper and lower depositional packages, distinct differences emerge in the distribution of channel–storey contact types (Fig. 7B and C). The lower section has an average of 16.7% C-C contacts, 52.2% C-H contacts and 13.9% C-F contacts, while the upper section has a more even distribution of contact types, with an average of 36.0% C-C contacts, 31.1% C-H contacts and 32.9% C-F contacts. In terms of areal distribution, the lower section hosts 14 outcrops demonstrating ≥50% C-H contacts, and the remaining nine outcrops are divided between hosting ≥50% C-C (A, C, E and I), ≥50% C-F contacts (R), or hosting no majority contact type (G, K, N and Q). One notable exception to the proximal-C-C/C-F trend was found in outcrop B, which demonstrated 60% C-H contacts. In the upper section, only five outcrops were found to exhibit ≥50% C-H contacts (K, M, Q, T and W), while ten outcrops exhibited ≥50% C-C contacts, seven exhibited ≥50% C-F contacts, and only two had no contact types ≥50% (L and N).

Interpreting contact type distribution

Evidence from the Salt Wash shows that contact type changes moving downstream on fluvial fans. Specifically, the proximal zone of the Salt Wash is dominated by C-C and C-F contact types, whereas the distal zone is dominated by C-H types. Because channel storey contacts can be interpreted as avulsion style indicators (C-C, annexation; C-F, incision; C-H, progradation), this change in contact type suggests that the proximal Salt Wash channels were mostly annexational, at times followed by incision. In the distal zone, channels were emplaced predominantly via progradation.

Avulsion style also changed through time. Analysis of the lower half of the Salt Wash shows that progradational avulsions were generally dominant, with the exception of a proximal, annexation-dominated subregion near the apex (Fig. 7B). The distribution of annexation and incision indicators expanded in the upper part of the Salt Wash (Fig. 7C), is consistent with the interpretation of persistent, system-scale progradation by Owen *et al*. (2017). The predominance of C-F contacts in the most proximal part of the

Table 1. Salt Wash channel body characteristics.

Map symbol	Outcrop name	Coordinates (latitude/ longitude)	Characteristic number of storeys	Cumulative channel storey thickness (m)	% C-C contacts lower	% C-H contacts lower	% C-F contacts lower	% C-C contacts upper	% C-H contacts upper	% C-F contacts upper
A	Collette Cyn	37.553574°–111.494683°	5.0	41.0	50.0	0.0	0.0	0.0	0.0	100.0
B	50 Mile Cyn	37.287079°–111.058512°	13.0	97.0	0.0	60.0	20.0	12.5	25.0	62.5
C	Bullfrog	37.662588°–110.808635°	10.5	121.8	54.5	27.3	0.0	66.7	33.3	0.0
D	Henries	38.100215°–110.634580°	10.5	55.3	37.5	62.5	0.0	61.5	15.4	23.1
E	Caineville	38.279346°–111.116298°	6.0	45.6	0.0	0.0	66.7	66.7	0.0	33.3
F	Hanksville	38.372755°–110.764618°	8.0	35.0	25.0	50.0	0.0	100.0	0.0	0.0
G	Butler Wash	37.480165°–109.617927°	9.5	85.4	40.0	0.0	40.0	11.1	0.0	88.9
H	Hatt's Ranch	38.877999°–110.372583°	6.0	42.8	0.0	100.0	0.0	50.0	25.0	25.0
I	Montezuma Cyn	37.786065°–109.270581°	11.5	64.2	58.3	16.7	8.3	9.1	0.0	90.9
J	Kane Springs	38.407596°–109.436248°	9.0	59.7	0.0	75.0	0.0	60.0	20.0	20.0
K	Buckhorn Flat	39.208753°–110.804140°	2.0	19.3	0.0	0.0	0.0	0.0	100.0	0.0
L	Woodside	39.199787°–110.398865°	4.5	26.2	0.0	100.0	0.0	28.6	42.9	28.6
M	Salt Valley	38.863785°–109.747975°	3.0	16.2	0.0	50.0	50.0	0.0	100.0	0.0
N	Slick Rock	38.044782°–108.895709°	10.0	58.2	36.4	45.5	0.0	44.4	33.3	22.2
O	McElmo Cyn	37.340864°–108.732206°	5.0	35.6	0.0	66.7	0.0	0.0	33.3	66.7
P	Dewey Bridge	38.821133°–109.297780°	10.0	51.7	30.0	50.0	20.0	60.0	20.0	20.0
Q	Polar Mesa	38.651850°–109.140322°	6.0	44.0	33.3	0.0	33.3	0.0	66.7	33.3
R	Atkinson Creek	38.395410°–108.751010°	8.5	63.0	0.0	37.5	62.5	33.3	0.0	66.7
S	Pinon	38.228651°–108.357696°	9.0	43.8	20.0	60.0	20.0	50.0	25.0	25.0
T	CO. NM	39.071045°–108.728457°	4.0	16.3	0.0	100.0	0.0	50.0	50.0	0.0
U	Bangs Cyn	38.980697°–108.602776°	1.5	14.2	0.0	100.0	0.0	100.0	0.0	0.0
V	Dominguez Cyn	38.395410°–108.751010°	5.0	18.9	0.0	100.0	0.0	25.0	25.0	50.0
W	Smith Fork	38.740581°–107.808604°	8.0	34.4	0.0	100.0	0.0	0.0	100.0	0.0
		Averages	**7.2**	**47.4**	**16.7**	**52.2**	**13.9**	**36.0**	**31.1**	**32.9**

Map symbol, outcrop name and coordinates are provided for each study location. Characteristic number of storeys refers to an average number of storeys across clusters, when more than one was present (see text for details). Cumulative channel thickness refers to the total thickness of channel bodies at each location. Percentages are given for each outcrop across all clusters. See Figs S1 to S12 for photographic panels representing outcrop analysis. Data for Collette Canyon, 50 Mile Canyon, Buckhorn Flat, Salt Valley, McElmo Canyon, Polar Mesa and Pinon are derived from data from Owen *et al*. (2015b).

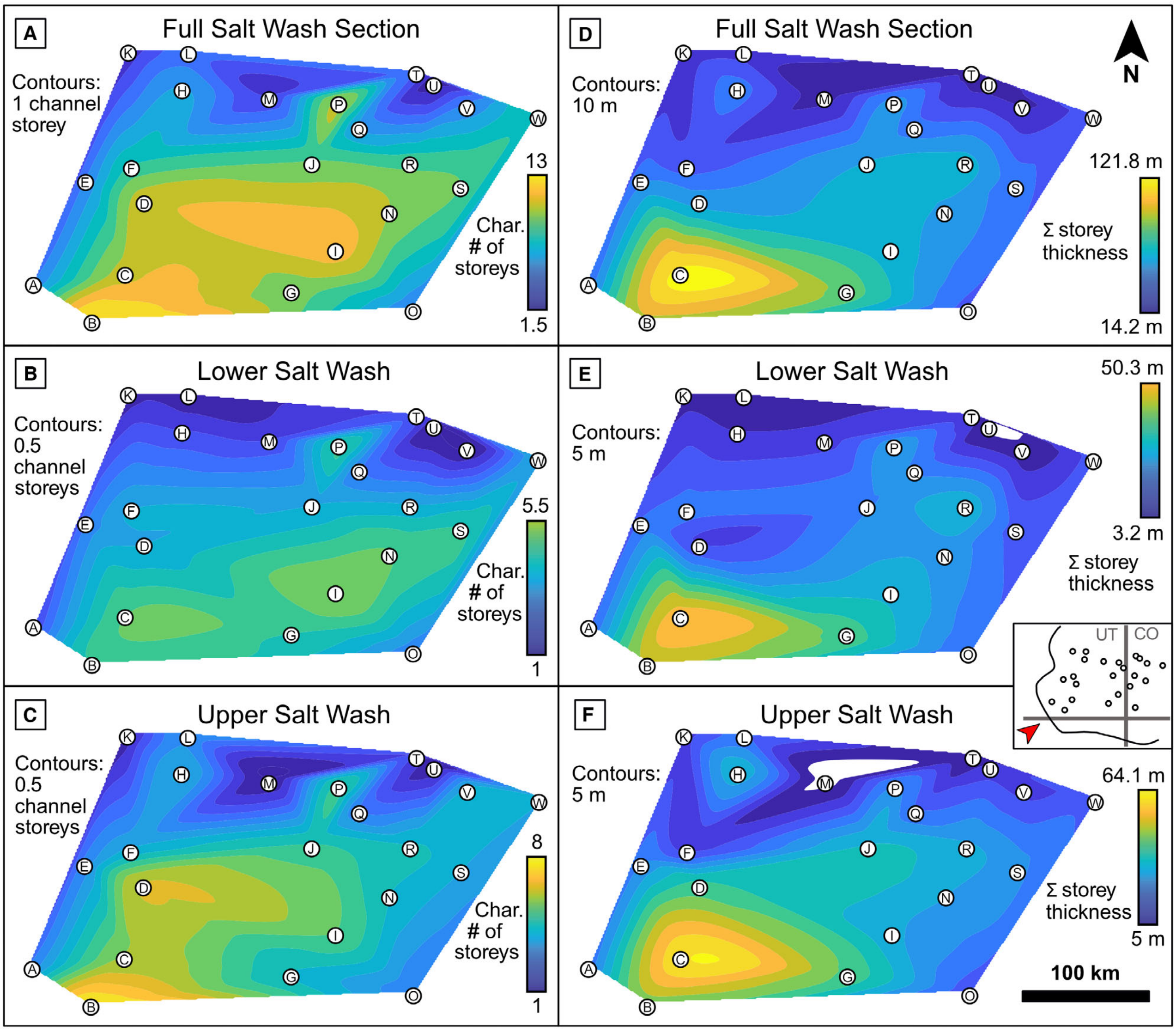

Fig. 5. Channel storey distribution and cumulative thickness. (A) to (C). Characteristic number of channel storeys at each study location. (D) to (F). Cumulative (Σ) storey thickness (in metres) at each study location. See Fig. 2 for geographic positions of study locations.

upper section (Fig. 7C, locations A and B) may represent sediment bypass (Owen *et al.*, 2015b), during which C-C storey contacts are reworked beyond recognition. Towards the south-east of the proximal upper section, the predominance of C-F contacts (locations I, G and O), may reflect a setting laterally offset from the system axis. Indeed, these outcrops correspond to significantly finer grain sizes and thinner section thicknesses mapped by Owen *et al.* (2015b, see Fig. 7C and E), as compared to a centrally located region hosting the largest grain sizes and thickest sections, corresponding to proximal upper-section outcrops this study found to be dominated by C-C contacts.

Changes in avulsion style must be inferred from contact types recorded in the stratigraphic record of the Salt Wash system. This interpretation carries inherent ambiguity, as outlined in previously described methods. Thus, numerical modelling of fluvial fan formation and remote sensing analysis of modern fan systems were employed to further explore the relationship between contact type and avulsion style, as well as how avulsion behaviour changes downstream.

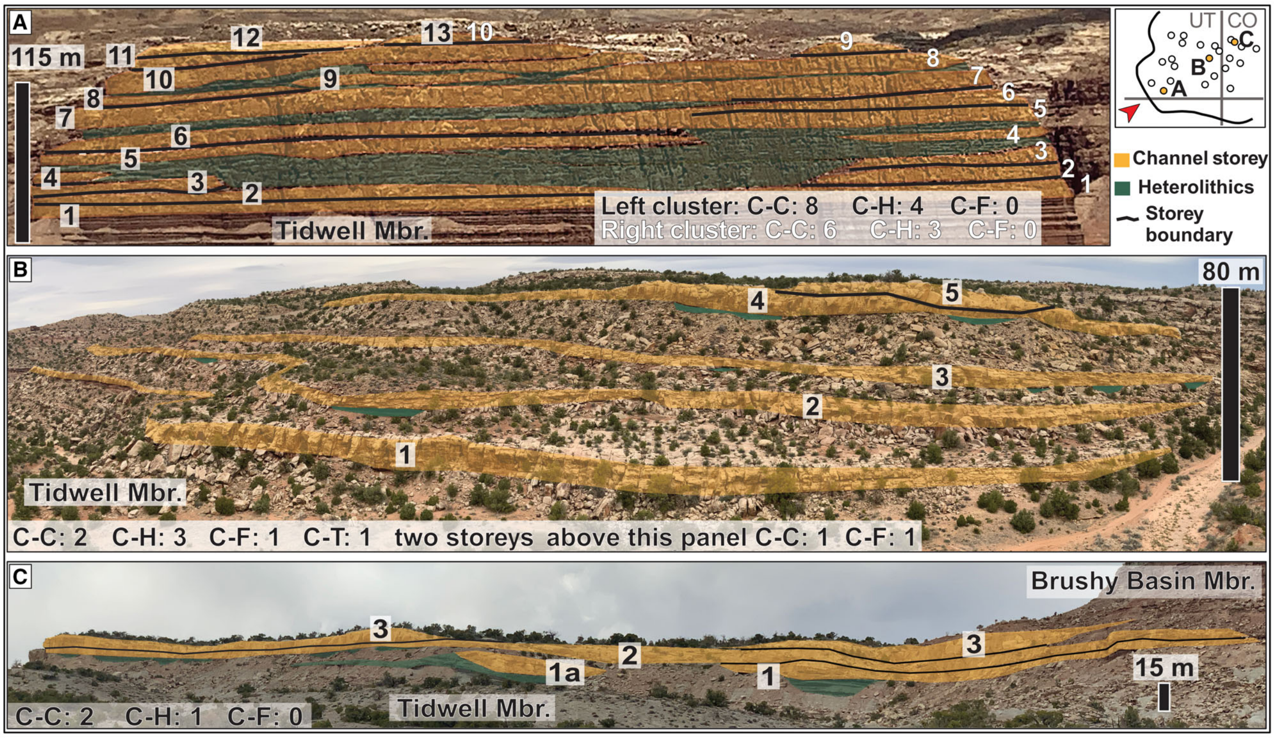

Fig. 6. Annotated outcrop panels in proximal, medial and distal locations. (A) Bullfrog outcrop (location C). Note all channel contacts are either channel–channel or channel–heterolithic, with no observed channel–floodplain contacts. This may reflect relatively coarser sediment among all facies in proximal settings, including floodplain deposits, rather than frequent progradational activity. (B) Kane Springs outcrop (location K). Note that two channel bodies were identified stratigraphically above this outcrop, not shown. C-T: 1 indicates that the first storey in this outcrop made contact with Tidwell Member strata and was not used in further contact-type analysis. (C) Bangs Canyon (location U). Note that this outcrop exhibited exceptionally sparse channel sandstone bodies, such that more than half of outcrop faces had none. To account for this during contact-type analysis, counts were halved (i.e. C-C: 1, C-H: 0.5, and C-F: 0).

NUMERICAL MODELLING AND REMOTE SENSING

Stratigraphic data suggests that avulsion style changes downstream, but it is difficult to determine the cause of this trend from stratigraphic data alone. To gain more insight into what causes this change, stratigraphic field results were compared to a cellular model of fluvial fan landscape evolution and to remotely-sensed avulsions on modern fans. The numerical model simulates alluvial topography and avulsion dynamics over large spatial (>100 km) and temporal (10^6 year) scales (Martin & Edmonds, 2022). For this comparison, two million years of fan development were simulated using the same parameters as fig. 6 in Martin & Edmonds (2022), except for healing direction, which was set such that abandoned channel bottoms and levées annealed towards one another (Martin & Edmonds, 2023). Channels in the model are subgrid cell features and avulsion can occur wherever channels are superelevated relative to the adjacent floodplain or abandoned channel and possess a gradient advantage. In a timestep when an avulsion trigger occurs (defined with a fixed probability), the avulsion location is chosen randomly from active channel cells that meet these criteria. The selected avulsion will then develop a new channel pathway, or pathfind, across unchannelized floodplain by a slope-weighted random walk (Edmonds *et al.*, 2016). While this process simulates progradation of the avulsion channel, here the term pathfinding is used in place of progradation, as no overbank deposition is simulated by the model.

Pathfinding continues until either the avulsion channel reaches the downstream exit of the domain, or it annexes or reoccupies an abandoned channel. These avulsion outcomes were interpreted as corresponding to specific channel storey contacts: pathfinding over unchannelized

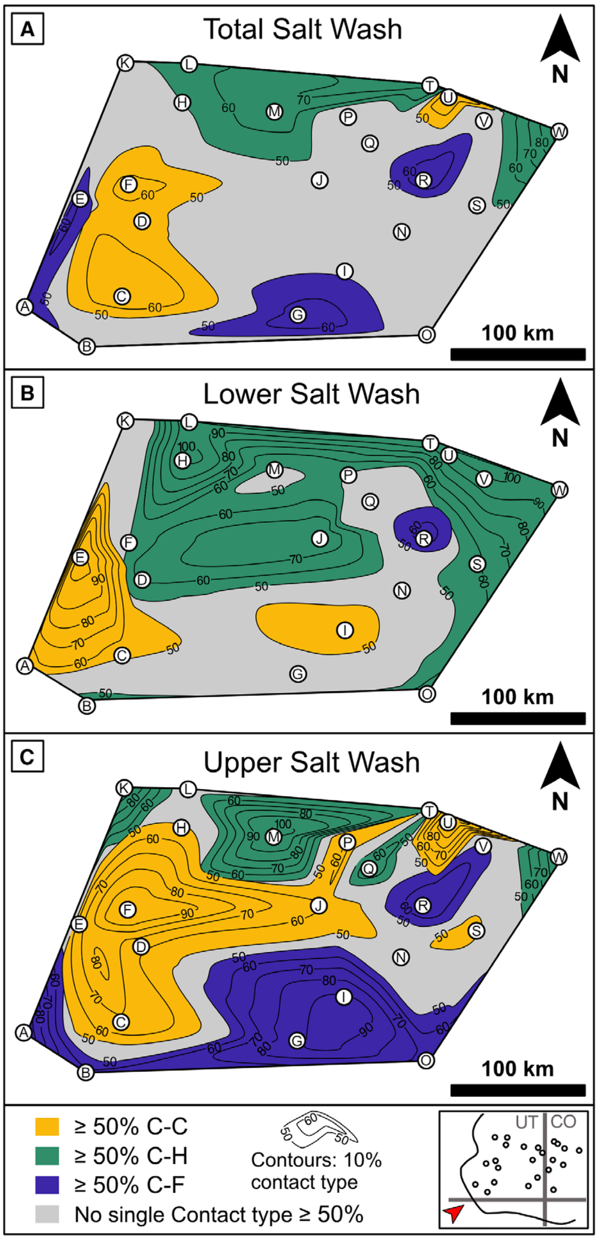

Fig. 7. Distribution of channel storey contact types. Contour lines show the percentage of the most dominant contact type at each outcrop. Colour indicates the contact type: yellow for ≥50% C-C contacts, green for ≥50% C-H contacts and blue for ≥50% C-F contacts. Grey areas indicate outcrops with no dominant (≥50%) channel-storey contact type. (A) Total Salt Wash section. (B) Lower half and (C) Upper half of Salt Wash section.

floodplain is interpreted to correspond with C-H or C-F channel storey contacts, while reoccupation is interpreted to correspond to C-C contacts. The model is unable to distinguish between C-H and C-F contact types because near-channel heterolithic sedimentation is not resolved. For each avulsion, the pathfinding distance was measured from the initiation site to either the reoccupation site or the downstream model boundary. These distances were attributed to the cells from which avulsions initiated, after which distances were averaged for each row. Measurements taken prior to fan formation (from the first 10% of model simulation time) were discarded.

Data from modern river systems were derived from the remote-sensing dataset of Valenza *et al.* (2020). This dataset includes a collection of avulsion events on foreland basin fluvial fans, captured in the Landsat archive from 1986 to 2017. For each event, Valenza *et al.* (2020) identified the spatial extent of avulsion-related floodplain disturbance and mapped the progression of avulsion activity across the floodplain. For the purposes of this work, avulsion events were subsampled from the Llano and Beni–Mamore basins within the Andean foreland. Due to differences in tectonic and climatic settings, these events do not provide perfect analogues to Salt Wash avulsions; the Salt Wash system has been interpreted as having developed in a distal forebulge to backbulge foreland setting, while the modern Andean systems are located in high-accommodation, proximal foreland settings, including wedge-top and foredeep depozones (DeCelles & Giles, 1996; Horton & DeCelles, 1997; Roddaz *et al.*, 2009). However, these modern avulsions are considered reasonable analogues to the Salt Wash since all compared avulsions occur in foreland basins and fans shared similar-scaled extents (*ca* 150 km from apex to toe). As for climatic settings, the Salt Wash has been interpreted as having developed in a semi-arid palaeoclimate, which fostered well-drained floodplains (Demko *et al.*, 2004; Weissmann *et al.*, 2013), as compared to the humid climate of the Llanos and Beni–Mamore basins, which creates poorly drained floodplains, parts of which remain inundated for months each year (Blydenstein, 1967; Seiler *et al.*, 2013). While it is difficult to characterize how these differences might limit comparison, the observations from Valenza *et al.* (2020) represent the only dataset of remotely sensed fluvial fan avulsions, and the authors have no *a priori* reason to expect completely different avulsion behaviour.

Simulations of fluvial fan formation

The fluvial fan model simulates avulsion behaviour, which is used to identify potential controls on the distribution of channel–storey contact types. The model forms a fan as sediment supplied to the top of the model domain accumulates in a basin in which subsidence decreases linearly downstream (Fig. 8). More specifically, sediment enters the domain from a point source, and concentrated deposition near the system apex results in high rates of avulsion. Over the course of two million years, repeated avulsions lead to the development of two characteristic features of fluvial fans: a radially divergent distribution of channels and a conical topography (Fig. 8A to C). Across the surface of the fan, flow and transport are generally distributive. In the basin beyond the elevated fan surface, channels exiting the fan toe switch from a radial regime to a convergent one, forming an apron of fluvial activity. While avulsions still occur on the fluvial apron, they are much less frequent than on the fan. These different domains of divergence and convergence match observations from modern fans (Fig. 1) (Hartley *et al*., 2010; Weissmann *et al*., 2011; Davidson *et al*., 2013).

For each simulated avulsion, the pathfinding distance was measured and used as a proxy for the possible extent and distribution of C-H contacts. In the proximal part of the domain on the fan surface, pathfinding channels travelled an average of *ca* 1.2 km (*ca* 2.5 cells) before encountering and annexing an abandoned channel (Fig. 8C). Conversely, avulsions occurring on the fluvial apron exhibited significantly longer pathfinding distances, with an average of 3.63 km (*ca* 7 cells). This occurs because abandoned channels are more widely dispersed on the apron, as compared to the fluvial fan, which is primarily composed of abandoned channels (Martin & Edmonds, 2022, 2023).

In this initial simulation (Fig. 8A to C), it seems that the downstream change in avulsion behaviour is caused by a downstream decrease in the distribution density of abandoned channels on the floodplain, which increases the distance between avulsion initiation sites and abandoned channels available for annexation. To test this idea, a second simulation with identical conditions as the first was set up, with an exception for setting a rule that prevented the reoccupation of abandoned channels so that avulsing channels ignore relict channels and continue pathfinding until they reach the end of the domain (Fig. 8D to F). This might occur, for instance, if channels fill with sediment during abandonment such that they do not attract future pathfinding rivers. When reoccupation is prevented in this way, the topography of the modelled fan looks remarkably like the first simulation, but significant differences emerge in the distribution of avulsion pathfinding distances. Rather than forming distinct zones hosting either short or long pathfinding distances (as in the first simulation), in this run, pathfinding distances demonstrate a relatively consistent downstream reduction from fan apex to the end of the modelled apron, reflecting the decreasing distance between the avulsion initiation site and the downstream domain boundary (Fig. 8D to F).

It is suggested that the downstream increase in avulsion pathfinding distance results from reduced densities of abandoned channels on the fluvial apron. This relationship is highlighted by the difference between runs that allowed or prohibited the reoccupation of abandoned channels. While the model does not simulate stratigraphic architecture, this avulsion behaviour should create stratigraphic indicators like those observed in the Salt Wash. Namely, avulsion events on the fan often annex adjacent relict channels, which should result in C-C contact types and amalgamated channel belts. Conversely, avulsion events on the apron traverse longer distances across the floodplain before encountering an abandoned channel; this would result in C-H contact types and heterolithic packages deposited from prograding crevasse splay networks. If an avulsion resulted in the annexation of a similar or smaller channel, it may incise through any channel fill to erase stratigraphic evidence of the pre-existing channel, resulting in a C-F contact.

Modern analogues from the remote-sensing record

The presented stratigraphic analysis and numerical modelling both suggest that avulsions change behaviour moving downstream from the fan surface to the fan apron. To further investigate this in modern systems, this study looked at the remote sensing record from Valenza *et al*. (2020). That study quantified avulsion style by measuring the surface area of avulsion-disturbed floodplain and dividing it by the parent channel surface area, thus yielding an avulsion-style ratio. In this scheme, annexational avulsions that reoccupy an existing channel with little to no floodplain disturbance and have an approximate 1 : 1 ratio. Conversely, progradational avulsions disturb substantial

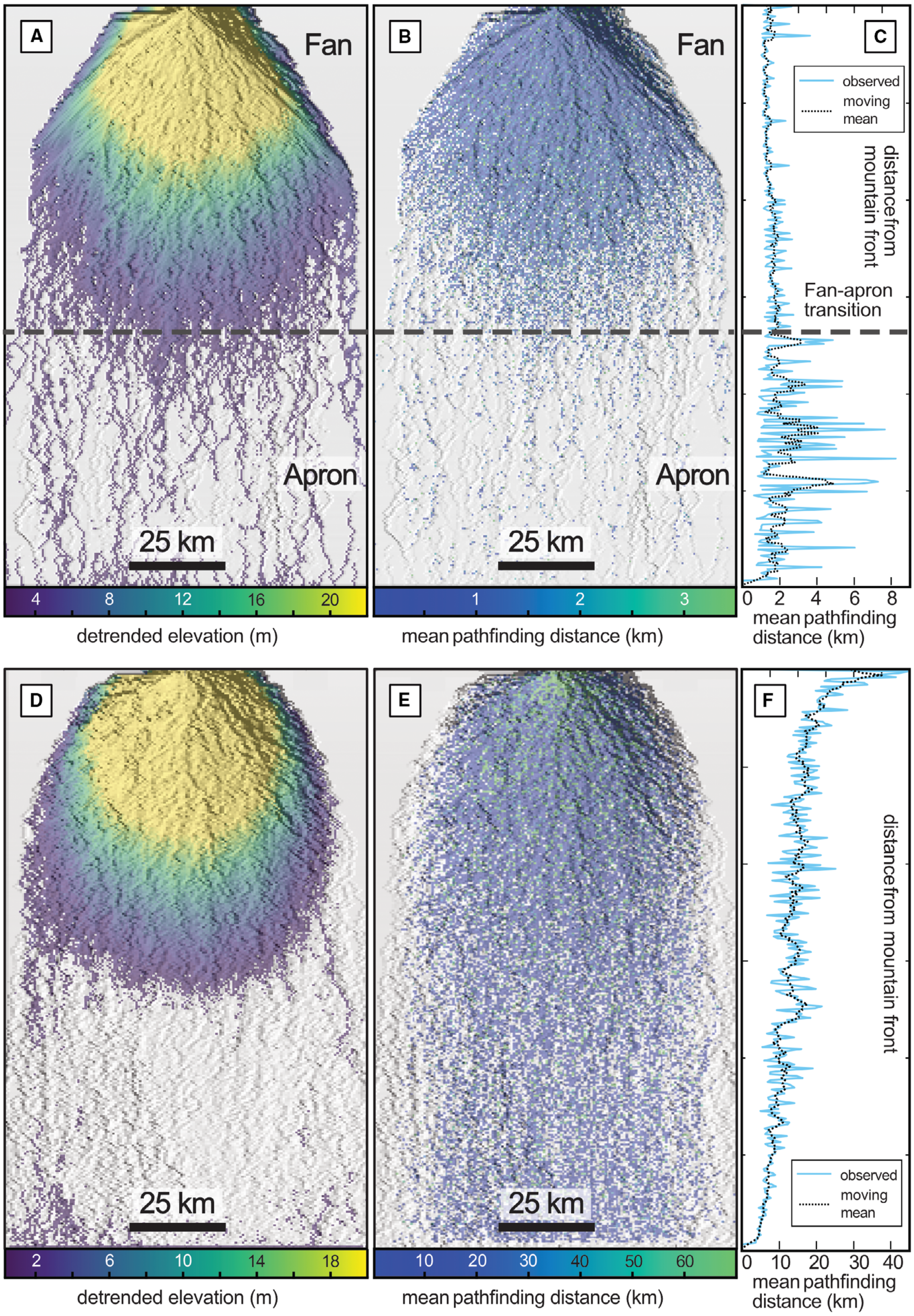

Fig. 8. Cellular fluvial fan model results. (A) and (D). Topography generated by channel avulsion over two million years. Elevation is detrended to account for regional slope in basin elevation moving away from the mountain front. (B) and (E). Mean pathfinding distance of avulsion events, a proxy for progradation, based on location of avulsion initiation. (C) and (F). Mean pathfinding distance of avulsion events moving downslope. Moving mean window is 2.5 km. Total length of modelled systems, from fan apex (top) through apron (bottom) of all panels, is 150 km. Panels (A) to (C) depict the model run that allows pathfinding avulsions to reoccupy abandoned channels, while panels (D) to (F) depict a scenario in which reoccupation is prevented.

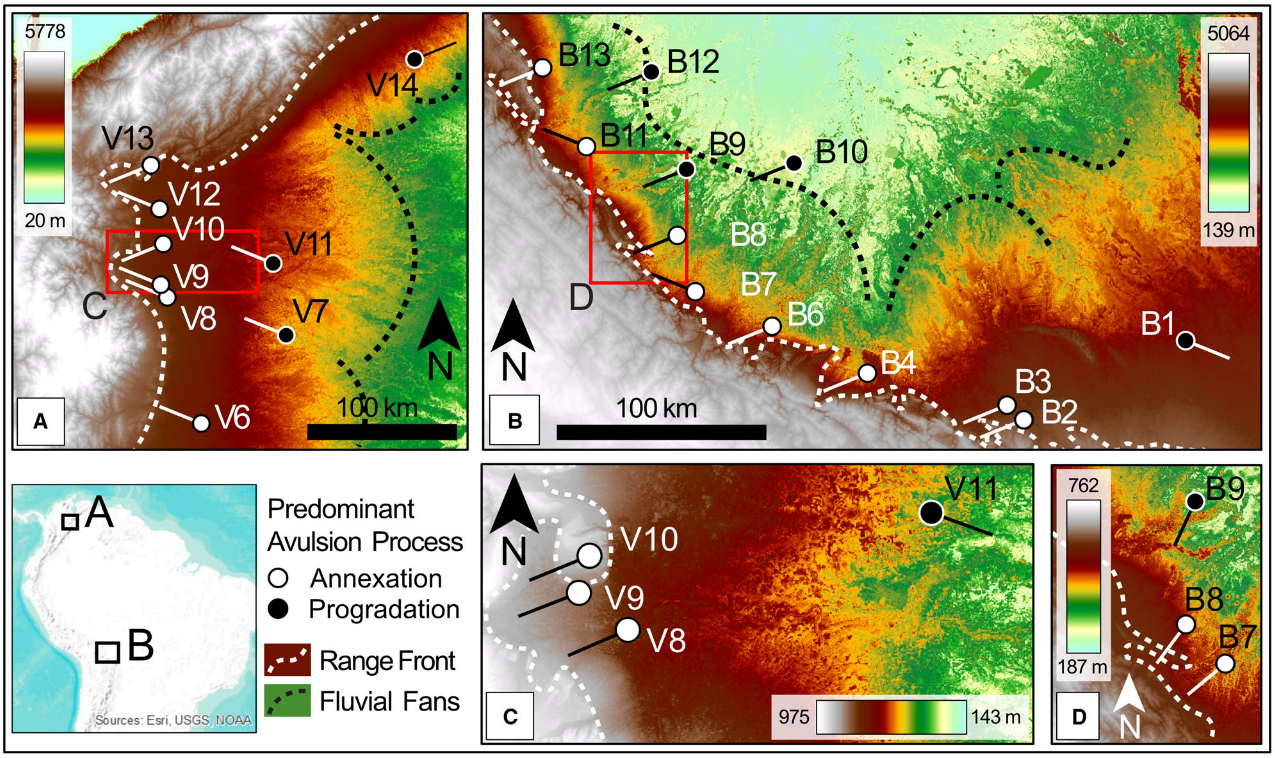

Fig. 9. Distribution of avulsion processes in Andean foreland basins. White dashed lines indicate the Andean range front/foreland basin margin. Black dashed lines indicate fluvial fan systems feeding into foreland basin. (A) Avulsion events in Venezuela and Colombia. (B) Avulsions in Bolivia. (C) Close-up of four avulsion events along Venezuela and Colombian border. (D) Close-up of three avulsion events in Bolivia. Digital elevation model (DEM) from O'Loughlin *et al.* (2016).

portions of the local floodplain, yielding ratios of at least 2.5, with the largest exceeding 30. Out of that dataset, 14 avulsions with ratios <2.5 (i.e. annexational) and seven with ratios >2.5 (i.e. progradational) were specifically looked at.

Fan surfaces hosted exclusively annexational avulsions (Fig. 9, avulsions V8–V10, and B7–B8). Moving downstream and farther from system apices, avulsions displayed increasing signs of progradation (Figs 9 and 10), including crevasse splays, ponds and distributary networks, which would theoretically deposit heterolithic sediment packages (Smith *et al.*, 1989; Smith & Perez-Arlucea, 1994; Slingerland & Smith, 2004; Davidson *et al.*, 2013; Valenza *et al.*, 2022).

Remote sensing also allows a clear view of how the avulsion behaviour of a single event varies in space, something that is nearly impossible to do in a stratigraphic cross-section. Valenza *et al.* (2022) showed that avulsions dominated by progradational processes typically contain one or more reaches of annexation. Examples from modern avulsions demonstrate that there can be multi-kilometre, alternating reaches dominated by annexation or progradation, which in some cases may produce a variety of stratigraphic avulsion indicators (Fig. 10). This suggests that avulsion style for a single channel depends on which reach of the avulsion belt is exposed. For this reason, any analysis of avulsion indicators should consider the average or characteristic distribution of features and their characteristics through time and space. This holistic approach is consistent with the field methodology presented here – averaging contact-type counts for locations that exhibited multiple, overlapping clusters of channel sandstone bodies, and investigating regional, rather than local trends.

Overall, what was observed in the remote sensing record is qualitatively consistent with observations from the Salt Wash and from numerical modelling. The remote sensing data show that avulsions occurring further downstream on fluvial fans demonstrate more progradation (Figs 9 and 10). Although remote sensing

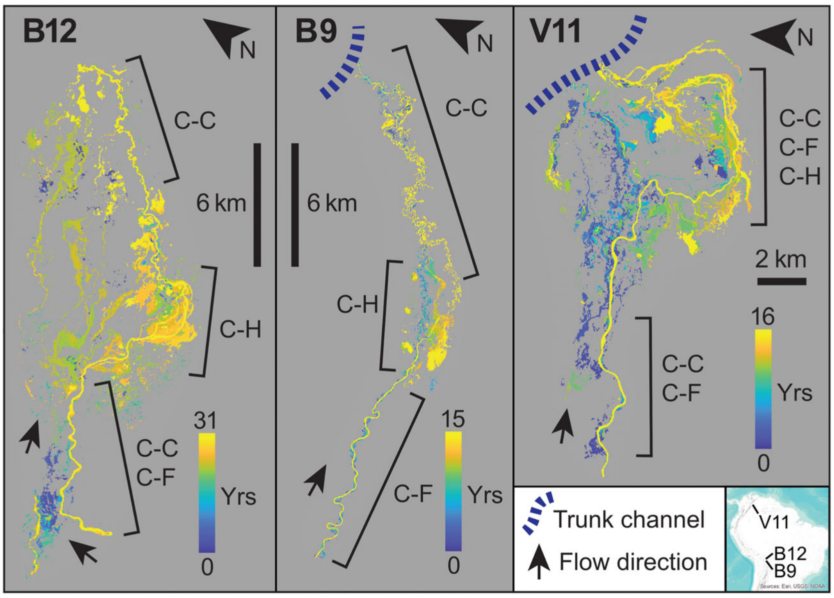

Fig. 10. Time-transgressive maps of avulsion activity, or avulsion fingerprints (after Valenza *et al.*, 2020). Fingerprints are made using a spectral compression of Landsat imagery (tasselled-cap transformation; Kauth & Thomas, 1976) with each colour representing a year's worth of avulsion activity. Warmer colours represent more recent activity. Blue dashed lines represent the trunk channel, the event eventually joined. Despite representing progradational avulsion events (Valenza *et al.*, 2020, 2022), each demonstrates a variety of avulsion processes, including reaches that would likely produce channel–channel (annexation), channel–floodplain (annexation followed by channel enlargement), and channel–heterolithic (progradation) contacts. Note the geographic locations of these events (B12, B9 and V11) are marked in Fig. 9.

does not measure deposition, the patterns of floodplain disturbance indicate the creation of crevasse splays and distributary networks. These are the fundamental elements of progradational avulsions and would likely create heterolithic deposits analogous to those of the Salt Wash.

LINKING DOWNSTREAM CHANGES IN AVULSION STYLE TO FLUVIAL ARCHITECTURE

The results presented here from outcrop stratigraphy, numerical modelling and remote sensing together support the hypothesis that changing avulsion style results in proximal to distal changes in stacking patterns of floodplain and channel-belt facies (Fig. 11). Returning to the example of the Salt Wash Member of the Morrison Formation, it is suggested that a downstream change in avulsion style is expressed as a change from amalgamated multi-storey channel sandstone bodies with little intervening fine-grained floodplain deposition (i.e. 'channel-dominated' stratigraphy) to more isolated channel sandstone bodies encased in floodplain muds (i.e. 'floodplain-dominated'; Owen *et al.*, 2015b, 2017). This kind of downstream change with no intervening unconformity is not unique to the Salt Wash and has been documented in other formations (see review in Heller *et al.*, 2015). Many different autogenic and allogenic explanations have been advanced to explain this type of change, such as variations in fluvial style from braided to meandering, subsidence, water or sediment supply, and base-level (Allen, 1978; Heller & Paola, 1996; Robinson & McCabe, 1997; Gibling, 2006; Weissmann *et al.*, 2013; Heller *et al.*, 2015). Analysis suggests that the downstream transition from channel-dominated to floodplain-dominated stratigraphy corresponds to a transition in avulsion style that also marks the boundary between the fluvial fan and apron.

The classic interpretation of this kind of architectural change usually suggests that the channel-dominated, amalgamated proximal deposits represent braid belts, and the floodplain-encased channels in the distal deposits are meandering rivers. However, Hartley *et al.* (2015) convincingly

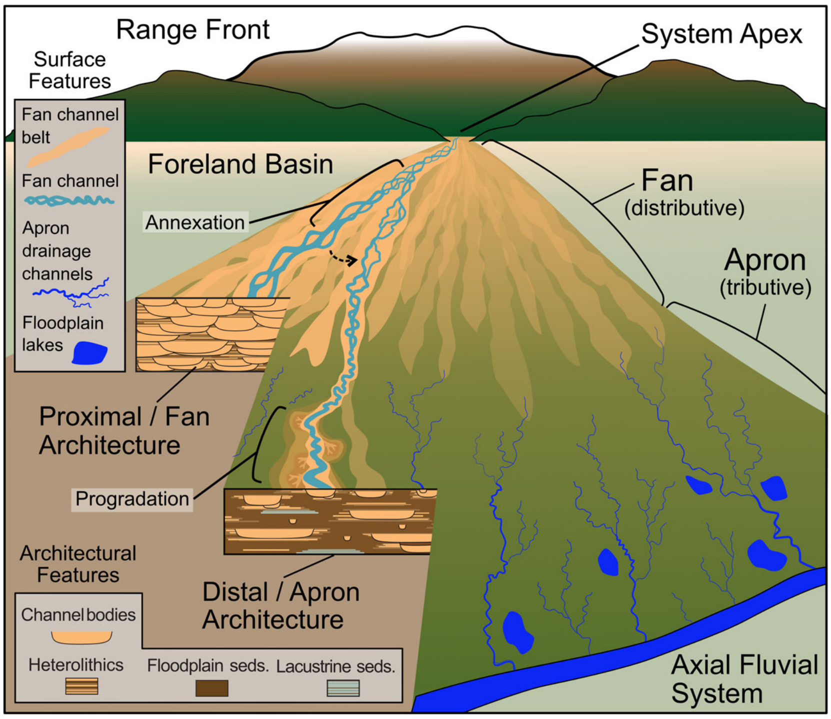

Fig. 11. Conceptual model of a fluvial fan–apron system. The proximal, distributive zone is modified by predominantly annexational avulsions, which set the primary channel pathway and create amalgamated, channel-dominated stratigraphy (predominantly C-C and C-F contacts). The broad, low-lying apron surface is scattered with local drainage channels that may attract regional avulsions. Because avulsions on the apron are less frequent and channels are spaced farther apart, avulsions prograde for significant distances before reoccupying another channel. Stratigraphy in this distal regime is mixed, but floodplain dominated (predominantly C-H, with minor C-F and C-C contacts). Note primary channel is depicted transitioning downstream from braided to meandering, after modern system example in Fig. 1.

showed that amalgamated, proximal Salt Wash channel deposits are correlative with plan view outcrops of meander loops and scroll bars, which are among the most reliable indicators of channel meandering. Thus, for this system, a change in channel planform morphology as driving the architectural change can be ruled out. Instead, data suggest that fluvial fan-apron architecture is shaped by avulsion behaviour. The amalgamated channel sandstone bodies with internal C-C storey contacts are interpreted as evidence of annexation-dominated fan environments (Figs 4A, 7 and 11). Downstream, channel sandstone bodies become less amalgamated, increasingly single-storeyed, and increasingly dominated by C-H contacts. Taken together, they indicate a fluvial apron environment, marked by a significantly greater dispersion of abandoned channels, and where avulsing flow must cross larger expanses of floodplain before reaching a channel suitable for reoccupation.

The important question that emerges is why avulsion style changes downstream. The stratigraphic data, numerical modelling and remote sensing all suggest that annexation is dominant on the fan, and progradation becomes increasingly dominant on the fluvial apron. Thus, it seems likely that a key factor is the number and distribution of abandoned channels on the floodplain. It is thought that there are two important mechanisms that determine the distribution density of abandoned channels. First, there are more frequent avulsions on the fan compared to the fluvial apron, which is the primary mechanism in creating the fan. It is commonly observed in the modern record that fluvial fan surfaces host abundant palaeochannels (Fig. 1) (Hartley *et al.*, 2010; Weissmann *et al.*, 2010; Martin & Edmonds, 2022). Using the same fan model, Martin & Edmonds (2023) showed that avulsions occur much more frequently on the fan surface than the apron. Frequent avulsions yield more abandoned channels, and rapid channel switching prevents the infill of channels with sediment. Avulsions are more frequent in the proximal reach due to a large sediment load and relatively rapid bed aggradation [Fig. 9 shows more proximal (black markers) than distal (white markers) avulsions within the Landsat record]. Second, the fan spreads radially from a point source, which increases the average distance between abandoned channels. In a radially expanding fan, if the number of abandoned channels moving down the fan were constant, the average distance between channels would increase as the fan widens. This would make progradational avulsions more common downstream where the spacing between channels is larger and avulsions must travel further before encountering abandoned channels. Furthermore, Martin & Edmonds (2023) showed that fluvial fans can show a reduction in the number of abandoned channels moving away from the mountain front, which amplifies this spacing effect even more.

Owen *et al.* (2015b) interpreted the Salt Wash Member (Fig. 2A) as a distributive fluvial system, and the downstream facies shift as resulting from a radially expanding fan and a downstream decrease in energy and discharge. Based on the present analysis, the channel-dominated extents of the Salt Wash are interpreted as fluvial fan deposits, and the floodplain-dominated extents as fluvial–apron deposits. These facies became stacked over time as the fan prograded into the basin, as described by Weissmann *et al.* (2013). This would explain the differences in channel–storey contact type, and thus avulsion processes, recorded in the lower and upper halves of Salt Wash stratigraphy (Fig. 7A and B). In the early phase, the fan would have had a limited extent, and most of the domain would have been dominated by the distal extent of the fan or fluvial apron, where avulsion activity was dominated by progradation. As the fan grew, it would have prograded over this distal apron, resulting in older stratigraphic architecture dominated by progradational avulsion indicators (distal fan to fluvial apron; Figs 7B and 11), and younger architecture dominated primarily by annexational indicators with secondary incisional indicators (fan-proper; Figs 7C and 11).

The analysis of modern, remotely sensed and numerically modelled avulsions implies that spatiotemporal stacking trends in channel sandstone bodies, as observed in the Salt Wash, can be explained by autogenic processes related to the avulsion behaviour of a prograding fluvial system (Fig. 11). Furthermore, results indicate that these trends can develop without requiring obvious stratigraphic changes in channel planform (braided or meandering) or allogenic drivers. This provides new perspectives on reconstructing the morphodynamic processes that shape fluvial stratigraphy and introduces a process-based definition of the fluvial fan versus the fan apron.

CONCLUSIONS

Through the integration of outcrop observations, numerical modelling and remote sensing analysis, this study underscores and characterizes the significance of avulsion behaviour on fluvial fan morphodynamics and stratigraphic architecture. The distribution of avulsion style indicators across the Salt Wash Member demonstrates a downstream transition from annexation to progradation, coinciding with a downstream change from amalgamated channel sandstone bodies to isolated ones. This downstream transition is consistent with remote-sensing imagery and numerical-model data, which depict annexation-prone fans densely covered by abandoned channels, and progradation-prone fluvial aprons hosting isolated abandoned channels, separated by expanses of floodplain. This downstream shift in avulsion style between fluvial fans and their aprons provides an autogenic channel-scale mechanism for the change in fluvial architecture observed in the Salt Wash. In a broader sense, these results suggest that downstream changes in avulsion style exert an important control on large-scale fluvial architecture and connectivity between channel sandstone bodies.

ACKNOWLEDGEMENTS

The authors gratefully acknowledge the generous sharing of coordinates for optimal Salt Wash study locations and additional stratigraphic data from Dr Amanda Owen, Senior Lecturer, University of Glasgow. Comments from the three external reviewers and the associate editor greatly improved this manuscript. The authors also gratefully acknowledge funding for this project from an International Association of Sedimentologists (IAS) Postgraduate Research Grant, a Geological Society of America (GSA) Graduate

Student Research Grant and National Science Foundation Grants 1911321 and 2321056. In addition, HKM was supported by NASA FINESST grant no. 80NSSC21K1598.

DATA AVAILABILITY STATEMENT

The data that supports the findings of this study are available in the supplementary material of this article.

REFERENCES

Allen, J.R. (1965) A review of the origin and characteristics of recent alluvial sediments. *Sedimentology*, **5**, 89–191.

Allen, J.R.L. (1978) Studies in fluviatile sedimentation: an exploratory quantitative model for the architecture of avulsion-controlled alluvial suites. *Sed. Geol.*, **21**, 129–147.

Allmendinger, R.W., **Miller, D.M.** and **Jordan, T.E.** (1984) Known and inferred Mesozoic deformation in the hinterland of the Sevier belt, northwest Utah. *Utah Geol. Assoc.*, **13**, 21–34.

Aslan, A., **Autin, W.J.** and **Blum, M.D.** (2005) Causes of river avulsion: insights from the late Holocene avulsion history of the Mississippi River, USA. *J. Sediment. Res.*, **75**, 650–664.

Blydenstein, J. (1967) Tropical savanna vegetation of the Llanos of Colombia. *J. Ecol.*, **48**, 1–15.

Bridge, J.S. and **Leeder, M.R.** (1979) A simulation model of alluvial stratigraphy. *Sedimentology*, **26**, 617–644.

Bryant, M., **Falk, P.** and **Paola, C.** (1995) Experimental study of avulsion frequency and rate of deposition. *Geology*, **23**, 365–368.

Chamberlin, E.P. and **Hajek, E.A.** (2015) Interpreting paleo-avulsion dynamics from multistory sand bodies. *J. Sediment. Res.*, **85**, 82–94.

Chamberlin, E.P., **Hajek, E.A.** and **Trampush, S.M.** (2016) Measuring Scales of autogenic organization in fluvial stratigraphy: An example from the Cretaceous Lower Williams Fork Formation, Colorado. In: *Autogenic Dynamics and Self-Organization in Sedimentary Systems* (Eds Budd, D.A., Hajek, E.A. and Purkis, S.J.), **106**, 132–144. Society for Sedimentary Geology (SEPM), Tulsa, OK.

Corbett, M.J., **Fielding, C.R.** and **Birgenheier, L.P.** (2011) Stratigraphy of a Cretaceous coastal-plain fluvial succession: the Campanian Masuk Formation, Henry Mountains syncline, Utah, USA. *J. Sediment. Res.*, **81**, 80–96.

Craig, L.C., **Holmes, C.N.**, **Freeman, V.L.**, **Mullens, T.E.** and **Weir, G.W.** (1955) *Stratigraphy of the Morrison and Related Formations, Colorado Plateau Region: A Preliminary Report. Geological Survey Bulletin 1009-E*, 125–168. USGS, Reston, VA.

Currie, B.S. (1997) Sequence stratigraphy of nonmarine Jurassic–Cretaceous rocks, central Cordilleran foreland-basin system. *GSA Bull.*, **109**, 1206–1222.

Davidson, S.K., **Hartley, A.J.**, **Weissmann, G.S.**, **Nichols, G.J.** and **Scuderi, L.A.** (2013) Geomorphic elements on modern distributive fluvial systems. *Geomorphology*, **180**, 82–95.

DeCelles, P.G. (2004) Late Jurassic to Eocene evolution of the Cordilleran thrust belt and foreland basin system, western USA. *Am. J. Sci.*, **304**, 105–168.

DeCelles, P.G. and **Burden, E.T.** (1992) Non-marine sedimentation in the overfilled part of the Jurassic-Cretaceous Cordilleran foreland basin: Morrison and Cloverly Formations, central Wyoming, USA. *Basin Res.*, **4**, 291–314.

DeCelles, P.G. and **Currie, B.** (1996) Long-term sediment accumulation in the Middle Jurassic–early Eocene Cordilleran retroarc foreland-basin system. *Geology*, **24**, 591–594.

DeCelles, P.G. and **Giles, K.A.** (1996) Foreland basin systems. *Basin Res.*, **8**, 105–123.

Demko, T.M., **Currie, B.S.** and **Nicoll, K.A.** (2004) Regional paleoclimatic and stratigraphic implications of paleosols and fluvial/overbank architecture in the Morrison Formation (Upper Jurassic), Western Interior, USA. *Sed. Geol.*, **167**, 115–135.

Dickinson, W.R. (2004) Evolution of the North American cordillera. *Annu. Rev. Earth Planet. Sci.*, **32**, 13–45.

Dickinson, W.R. (2006) Geotectonic evolution of the Great Basin. *Geosphere*, **2**, 353–368.

Dickinson, W.R. and **Gehrels, G.E.** (2008) Sediment delivery to the Cordilleran foreland basin: Insights from U-Pb ages of detrital zircons in Upper Jurassic and Cretaceous strata of the Colorado Plateau. *Am. J. Sci.*, **308**, 1041–1082.

Dickinson, W.R. and **Lawton, T.F.** (2001) Tectonic setting and sandstone petrofacies of the Bisbee basin (USA–Mexico). *J. S. Am. Earth Sci.*, **14**, 475–504.

Diemer, J.A. and **Belt, E.S.** (1991) Sedimentology and paleohydraulics of the meandering river systems of the Fort Union Formation, southeastern Montana. *Sed. Geol.*, **75**, 85–108.

Edmonds, D.A., **Hajek, E.A.**, **Downton, N.** and **Bryk, A.B.** (2016) Avulsion flow-path selection on rivers in foreland basins. *Geology*, **44**, 695–698.

Foreman, B.Z., **Heller, P.L.** and **Clementz, M.T.** (2012) Fluvial response to abrupt global warming at the Palaeocene/Eocene boundary. *Nature*, **491**, 92–95.

Gibling, M.R. (2006) Width and thickness of fluvial channel bodies and valley fills in the geological record: a literature compilation and classification. *J. Sediment. Res.*, **76**, 731–770.

Google Earth Pro. (2024) Arauca Province, Colombia [6.691150° N, 71.846373° W]. Landsat/Copernicus.

Hajek, E.A. and **Edmonds, D.** (2014) Is river avulsion style controlled by floodplain morphodynamics? *Geology*, **42**, 199–202.

Hajek, E.A. and **Wolinsky, M.A.** (2012) Simplified process modeling of river avulsion and alluvial architecture: connecting models and field data. *Sed. Geol.*, **257-260**, 1–30.

Hartley, A.J., **Owen, A.**, **Swan, A.**, **Weissmann, G.S.**, **Holzweber, B.I.**, **Howell, J.**, **Nichols, G.** and **Scuderi, L.** (2015) Recognition and importance of amalgamated sandy meander belts in the continental rock record. *Geology*, **43** (8), 679–682.

Hartley, A.J., **Weissmann, G.S.**, **Nichols, G.J.** and **Warwick, G.L.** (2010) Large distributive fluvial systems: characteristics, distribution, and controls on development. *J. Sediment. Res.*, **80**, 167–183.

Heller, P.L. and **Paola, C.** (1996) Downstream changes in alluvial architecture; an exploration of controls on channel-stacking patterns. *J. Sediment. Res.*, **66**, 297–306.

Heller, P., **Bowdler, S.**, **Chambers, H.**, **Coogan, J.**, **Hagen, E.**, **Shuster, M.**, **Winslow, N.** and **Lawton, T.** (1986) Time of initial thrusting in the Sevier orogenic belt, Idaho-Wyoming and Utah. *Geology*, **14**, 388–391.

Heller, P.L., **Ratigan, D.**, **Trampush, S.**, **Noda, A.**, **McElroy, B.**, **Drever, J.** and **Huzurbazar, S.** (2015) Origins of bimodal stratigraphy in fluvial deposits: an example from the Morrison Formation (Upper Jurassic), western USA. *J. Sediment. Res.*, **85**, 1466–1477.

Holbrook, J. (2001) Origin, genetic interrelationships, and stratigraphy over the continuum of fluvial channel-form bounding surfaces: an illustration from middle Cretaceous strata, southeastern Colorado. *Sed. Geol.*, **144**, 179–222.

Horton, B.K. and **DeCelles, P.G.** (1997) The modern foreland basin system adjacent to the Central Andes. *Geology*, **25**, 895–898.

Johnson, E.A. and **Pierce, F.W.** (1990) Variations in fluvial deposition on an alluvial plain: an example from the Tongue River Member of the Fort Union Formation (Paleocene), southeastern Powder River Basin, Wyoming, USA. *Sed. Geol.*, **69**, 21–36.

Jones, H. and **Hajek, E.A.** (2007) Characterizing avulsion stratigraphy in ancient alluvial deposits. *Sed. Geol.*, **202**, 124–137.

Jones, L. and **Schumm, S.** (1999) Causes of avulsion: an overview. In: *Fluvial Sedimentology VI* (Eds Smith, N.D. and Rogers, J.), 171–178. Wiley-Blackwell, Oxford.

Kauth, R.J. and **Thomas, G.** (1976) The tasselled cap-a graphic description of the spectral-temporal development of agricultural crops as seen by Landsat. In: *Symposium on Machine Processing of Remotely Sensed Data: Proceedings of the LARS Symposia* (Eds Swain, P.H., Morrison, D.B. and Parks, D.E.), pp. 41–51. The Laboratory for Applications of Remote Sensing, West Lafayette, IN.

Kowallis, B.J., **Christiansen, E.H.** and **Deino, A.L.** (1991) Age of the Brushy Basin Member of the Morrison Formation, Colorado Plateau, western USA. *Cretac. Res.*, **12**, 483–493.

Kowallis, B.J., **Christiansen, E.H.**, **Deino, A.L.**, **Peterson, F.**, **Turner, C.E.**, **Kunk, M.J.** and **Obradovich, J.D.** (1998) The age of the Morrison Formation. *Modern Geol.*, **22**, 235–260.

Kraus, M.J. and **Gwinn, B.** (1997) Facies and facies architecture of Paleogene floodplain deposits, Willwood Formation, Bighorn basin, Wyoming, USA. *Sed. Geol.*, **114**, 33–54.

Kraus, M.J. and **Wells, T.M.** (1999) Facies and facies architecture of Paleocene floodplain deposits, Fort Union Formation, Bighorn Basin, Wyoming. *Mt. Geol.*, **36**, 57–70.

Kraus, M., **Wells, T.**, **Smith, N.** and **Rogers, J.** (1999) Recognizing avulsion deposits in the ancient stratigraphical record. *Fluvial Sedimentol.*, **6**, 251–268.

Kumar, R. (1993) Coalescence megafan: multistorey sandstone complex of the late-orogenic (Mio-Pliocene) sub-Himalayan belt, Dehra Dun, India. *Sed. Geol.*, **85**, 327–337.

Labourdette, R. and **Jones, R.R.** (2007) Characterization of fluvial architectural elements using a three-dimensional outcrop data set: Escanilla braided system, South-Central Pyrenees, Spain. *Geosphere*, **3**, 422–434.

Leeder, M. (1977) A quantitative stratigraphic model for alluvium, with special reference to channel deposit density and interconnectedness.

Leleu, S., **Hartley, A.J.** and **Williams, B.P.** (2009) Large-scale alluvial architecture and correlation in a Triassic pebbly braided river system, lower Wolfville Formation (Fundy Basin, Nova Scotia, Canada). *J. Sediment. Res.*, **79**, 265–286.

Li, Y. and **Bhattacharya, J.** (2014) Facies architecture of asymmetrical branching distributary channels: Cretaceous Ferron Sandstone, Utah, USA. *Sedimentology*, **61**, 1452–1483.

Lynds, R. and **Hajek, E.A.** (2006) Conceptual model for predicting mudstone dimensions in sandy braided-river reservoirs. *AAPG Bull.*, **90**, 1273–1288.

Mackey, S.D. and **Bridge, J.S.** (1995) Three-dimensional model of alluvial stratigraphy; theory and applications. *J. Sediment. Res.*, **65**, 7–31.

Martin, H.K. and **Edmonds, D.A.** (2022) The push and pull of abandoned channels: how floodplain processes and healing affect avulsion dynamics and alluvial landscape evolution in foreland basins. *Earth Surf. Dyn.*, **10**, 555–579.

Martin, H.K. and **Edmonds, D.A.** (2023) Avulsion dynamics determine fluvial fan morphology in a cellular model. *Geology*, **51**, 796–800.

Millard, C., **Edmonds, D.A.** and **Hajek, E.A.** (2017) Evaluating the controls on crevasse-splay size: implications for floodplain-basin filling. *J. Sediment. Res.*, **87**, 722–739.

Mohrig, D., **Heller, P.L.**, **Paola, C.** and **Lyons, W.J.** (2000) Interpreting avulsion process from ancient alluvial sequences: Guadalope-Matarranya system (northern Spain) and Wasatch Formation (western Colorado). *Geol. Soc. Am. Bull.*, **112**, 1787–1803.

Morozova, G.S. and **Smith, N.D.** (2000) Holocene avulsion styles and sedimentation patterns of the Saskatchewan River, Cumberland Marshes, Canada. *Sed. Geol.*, **130**, 81–105.

Mullens, T.E. and **Freeman, V.L.** (1957) Lithofacies of the Salt Wash Member of the Morrison Formation, Colorado Plateau. *GSA Bull.*, **68**, 505–526.

O'Loughlin, F.E., **Paiva, R.C.D.**, **Durand, M.**, **Alsdorf, D.E.** and **Bates, P.D.** (2016) A multi-sensor approach towards a global vegetation corrected SRTM DEM product. *Remote Sens. Environ.*, **182**, 49–59.

Olsen, H. (1989) Sandstone-body structures and ephemeral stream processes in the Dinosaur Canyon Member, Moenave Formation (Lower Jurassic), Utah, USA. *Sed. Geol.*, **61**, 207–221.

Owen, A., **Jupp, P.E.**, **Nichols, G.J.**, **Hartley, A.J.**, **Weissmann, G.S.** and **Sadykova, D.** (2015a) Statistical estimation of the position of an apex: application to the geological record. *J. Sediment. Res.*, **85**, 142–152.

Owen, A., **Nichols, G.J.**, **Hartley, A.J.**, **Weissmann, G.S.** and **Scuderi, L.A.** (2015b) Quantification of a distributive fluvial system: the Salt Wash DFS of the Morrison Formation, SW USA. *J. Sediment. Res.*, **85**, 544–561.

Owen, A., **Nichols, G.J.**, **Hartley, A.J.** and **Weissmann, G.S.** (2017) Vertical trends within the prograding Salt Wash distributive fluvial system, SW United States. *Basin Res.*, **29**, 64–80.

Perez-Arlucea, M. and **Smith, N.D.** (1999) Depositional patterns following the 1870s avulsion of the Saskatchewan River (Cumberland marshes, Saskatchewan, Canada). *J. Sediment. Res.*, **69**, 62–73.

Peterson, F. (1980) Sedimentology of the uranium-bearing Salt Wash Member and Tidwell unit of the Morrison Formation in the Henry and Kaiparowits basins, Utah. *Utah Geological Association Symposium*, 1980 Henry Mountains Symposium, 305–322.

Peterson, F. (1984) Fluvial sedimentation on a quivering craton: influence of slight crustal movements on fluvial processes, Upper Jurassic Morrison Formation, western Colorado Plateau. *Sed. Geol.*, **38**, 21–49.

Peterson, F. (1986) *Jurassic Paleotectonics in the West-Central Part of the Colorado Plateau, Utah and Arizona*. AAPG, AAPG Special Volumes.

Peterson, F. (1994) *Sand Dunes, Sabkhas, Streams, and Shallow Seas: Jurassic Paleogeography in the Southern Part of the Western Interior Basin*. Rocky Mountain Section (SEPM), Denver, 233–272 pp.
Platt, N.H. and **Keller, B.** (1992) Distal alluvial deposits in a foreland basin setting—the Lower Freshwater Miocene, Switzerland: sedimentology, architecture and palaeosols. *Sedimentology*, **39**, 545–565.
Robinson, J.W. and **McCabe, P.J.** (1997) Sandstone-body and shale-body dimensions in a braided fluvial system: Salt Wash Sandstone Member (Morrison Formation), Garfield County, Utah. *AAPG Bull.*, **81**, 1267–1291.
Robinson, J.W. and **McCabe, P.J.** (1998) Evolution of a braided river system: the Salt Wash Member of the Morrison Formation (Jurassic) in southern Utah. In: *Relative Role of Eustasy, Climate, and Tectonism in Continental Rocks* (Eds Shanley, K.W. and McCabe, P.J.), *SEPM Special Publication*, **59**, 93–107. The Society for Sedimentary Geology (SEPM), Tulsa, OK.
Roddaz, M., **Hermoza, W.**, **Mora, A.**, **Baby, P.**, **Parra, M.**, **Christophoul, F.**, **Brusset, S.** and **Espurt, N.** (2009) Cenozoic Sedimentary Evolution of the Amazonian Foreland Basin System. In: *Amazonia: Landscape and Species Evolution: A Look into the Past* (Eds Hoorn, C. and Wesselingh, F.P.), pp. 61–88. Wiley-Blackwell, Oxford.
Rust, B.R. and **Jones, B.G.** (1987) The Hawkesbury Sandstone south of Sydney, Australia; Triassic analogue for the deposit of a large, braided river. *J. Sediment. Res.*, **57**, 222–233.
Seiler, C., **Hutjes, R.W.** and **Kabat, P.** (2013) Climate variability and trends in Bolivia. *J. Appl. Meteorol. Climatol.*, **52**, 130–146.
Slingerland, R. and **Smith, N.D.** (1998) Necessary conditions for a meandering-river avulsion. *Geology*, **26**, 435–438.
Slingerland, R. and **Smith, N.D.** (2004) River avulsions and their deposits. *Annu. Rev. Earth Planet. Sci.*, **32**, 257–285.
Smith, N.D. and **Perez-Arlucea, M.** (1994) Fine-grained splay deposition in the avulsion belt of the lower Saskatchewan River, Canada. *J. Sediment. Res.*, **64**, 159–168.
Smith, N.D., **Cross, T.A.**, **Dufficy, J.P.** and **Clough, S.R.** (1989) Anatomy of an avulsion. *Sedimentology*, **36**, 1–23.
Spencer, J.E., **Richard, S.M.**, **Gehrels, G.E.**, **Gleason, J.D.** and **Dickinson, W.R.** (2011) Age and tectonic setting of the Mesozoic McCoy Mountains Formation in western Arizona, USA. *GSA Bull.*, **123**, 1258–1274.
Tunbridge, I.P. (1981) Sandy high-energy flood sedimentation—some criteria for recognition, with an example from the Devonian of SW England. *Sed. Geol.*, **28**, 79–95.
Turner, C.E. and **Fishman, N.S.** (1991) Jurassic Lake T'oo'dichi': a large alkaline, saline lake, Morrison Formation, eastern Colorado Plateau. *GSA Bull.*, **103**, 538–558.
Turner, C.E. and **Peterson, F.** (2004) Reconstruction of the Upper Jurassic Morrison Formation extinct ecosystem—a synthesis. *Sed. Geol.*, **167**, 309–355.
Tyler, N. and **Ethridge, F.G.** (1983) Depositional setting of the Salt Wash Member of the Morrison Formation, southwest Colorado. *J. Sediment. Res.*, **53**, 67–82.
Valenza, J.M., **Edmonds, D.A.**, **Hwang, T.** and **Roy, S.** (2020) Downstream changes in river avulsion style are related to channel morphology. *Nat. Commun.*, **11**, 2116.
Valenza, J.M., **Edmonds, D.A.** and **Weissmann, G.S.** (2022) Quantifying river avulsion activity from satellite remote sensing: Implications for how avulsions contribute to floodplain stratigraphy in foreland basins. *J. Sediment. Res.*, **92**, 487–502.
Weissmann, G., **Hartley, A.**, **Nichols, G.**, **Scuderi, L.**, **Olson, M.**, **Buehler, H.** and **Banteah, R.** (2010) Fluvial form in modern continental sedimentary basins: distributive fluvial systems. *Geology*, **38**, 39–42.
Weissmann, G., **Hartley, A.J.**, **Nichols, G.J.**, **Scuderi, L.**, **Olsen, M.** and **Buehler, H.** (2011) Alluvial facies distributions in continental sedimentary basins: distributive fluvial systems. *SEPM Special Publication*, **97**, 327–356.
Weissmann, G., **Hartley, A.**, **Scuderi, L.**, **Nichols, G.**, **Davidson, S.**, **Owen, A.**, **Atchley, S.**, **Bhattacharyya, P.**, **Chakraborty, T.** and **Ghosh, P.** (2013) Prograding distributive fluvial systems: geomorphic models and ancient examples. *SEPM Special Publication*, **104**, 131–147.

Manuscript received 13 October 2023; revision accepted 29 May 2024

Supporting Information

Additional information may be found in the online version of this article:

Figure S1. Additional outcrop photographic panels used in characterizing study locations.

Figure S2. Additional outcrop photographic panels used in characterizing study locations.

Figure S3. Additional outcrop photographic panels used in characterizing study locations.

Figure S4. Additional outcrop photographic panels used in characterizing study locations.

Figure S5. Additional outcrop photographic panels used in characterizing study locations.

Figure S6. Additional outcrop photographic panels used in characterizing study locations.

Figure S7. Additional outcrop photographic panels used in characterizing study locations.

Figure S8. Additional outcrop photographic panels used in characterizing study locations.

Figure S9. Additional outcrop photographic panels used in characterizing study locations.

Figure S10. Additional outcrop photographic panels used in characterizing study locations.

Figure S11. Additional outcrop photographic panels used in characterizing study locations.

Figure S12. Additional outcrop photographic panels used in characterizing study locations.

Table S1. Extended data from outcrop analyses.